Energetic and Exergetic Analysis of a Solar Organic Rankine Cycle with Triple Effect Absorption System

Moslem Sharifishourabi

Submitted to the
Institute of Graduate Studies and Research
in partial fulfillment of the requirements for the degree of

Master of Science
in
Mechanical Engineering

Eastern Mediterranean University
July 2016
Gazimağusa, North Cyprus

Approval of the Institute of Graduate Studies and Research

Prof. Dr. Mustafa Tümer
Acting Director

I certify that this thesis satisfies the requirements as a thesis for the degree of Master of Science in Mechanical Engineering.

Assoc. Prof. Dr. Hasan Hacışevki
Chair, Department of Mechanical Engineering

We certify that we have read this thesis and that in our opinion it is fully adequate in scope and quality as a thesis for the degree of Master of Science in Mechanical Engineering.

Prof. Dr. Uğur Atikol
Supervisor

Examining Committee

1. Prof. Dr. Uğur Atikol

2. Prof. Dr. İbrahim Sezai

3. Asst. Prof. Dr. Murat Özdenefe

ABSTRACT

As the population increases, the energy demand increases and this requires to develop new and alternative technologies such as wind, solar, biomass, and geothermal for meeting the demands. There was a significant increase in the study of multi-generation energy systems in the last decades, in order to decrease consumption of non-renewable energy sources and optimize more viable and economical energy production. A multi-generation system is a process used to produce three or more different outputs, such as hydrogen, electricity, cooling, hot water, heating, fresh air and water with the same input energy sources.

In this thesis, a new multi-generation energy system is proposed based on solar energy. Solar energy is applied by feeding an Organic Rankine Cycle (ORC) which is then used to supply hot water to the buildings as well as electric current to the electrolyser with the aim of production hydrogen and also using in the building. A triple effect absorption system is utilized to produce cooling, heating, and dry air.

A comprehensive thermodynamic analysis is defined, and the effects of various operating conditions and configurations on the output are analyzed. The results show that the system has an exergetic utilization factor of 0.6 and an energetic utilization factor of 2.61 based on generating electricity of 427kW. Also the energetic and exergetic COP of absorption chiller are determined to be 1.16 and 0.24, respectively. In the proposed system, the energetic and exergetic efficiency of Organic Rankine Cycle are 21.08% and 33.98, respectively. The extracted numbers from the system analysis in comparison with previous studies, validate the system performance under

the defined initial parameters. So by analyzing the obtained results, it has become a necessity to decrease the system's irreversibility and increase the energy and exergy efficiencies to reach a high efficient system. All modeling and thermodynamic analysis have been done by Engineering Equation Solver (EES) software.

Keywords: Absorption System, Multi-generation System, Energy, Exergy, Efficiency.

ÖZ

Dünya nüfusu arttıkça, enerji talebi artmakta ve gerekli rüzgar, güneş, biyokütle ve jeotermal gibi yeni alternatif enerji kaynakları ön plana çıkmaktadır. Ekonomik fizibilitesi daha uygun olan daha uygun ve ekonomik enerji üretimini optimize etmek için yenilenebilir olmayan enerji kullanımını azaltmak için kayda değer sayıda çalışmalar yapılmıştır. Çok üretimli sistemler tek bir enerji kaynağndan, hidrojen, elektrik, soğutma, sıcak su, ısıtma, taze hava ve su gibi üç veya daha çok çıktının sağlandığı bir işlemdir.

Bu tezde, güneş enerjisine dayalı çok üretimli yeni bir enerji sistemi önerilmektedir. Güneş enerjisi hidrojen üretimi amacıyla elektroliz kullanarak ve aynı zamanda binada kullanmak için bina ve elektrik sıcak su temini için bir Organik Rankine Çevrimini (ORC) beslemek için uygulanmıştır. Bir üçlü etkili abzorpsiyonlu sistem, soğutma ısıtma ve kuru hava üretmek için kullanılmıştır.

Kapsamlı bir termodinamik analizi tanımlanmş olup çıktılar üzerinde farklı işlem koşulları, etkileri ve konfigürasyonları analiz edildi. Sonuçlara göre sistemin elektrik üretim kapasitesi 427kW olduğunda, ekserjetik kullanım faktörü 0.6 olup enerji kullanım faktörü ise 2.61 dir. Ayrıca soğutma sistemine ait enerji ve ekserji COP değerleri sırasıyla 1.16 ve 0.24 olarak belirlenmiştir. Önerilen sistemde, enerjik ve ekserjetic verim Ornagik Rankine Cevriminde sirasiyla %21.08 ve %38.98 dir. Sistem analizlerinden elde edilen değerler daha önceki çalışmalarla karşılaştırıldığında sonuçların geçerli olduğu kanaatine varılmıştır. Ayrıca analizden elde edilen sonuçlarda, irreversibilitileri azaltmak ve verimlilikleri artırmak sureti ile

sistemi optimize etmek bir gereklilik olmuştur. Bütün modelleme ve termodinamik analizler Engineering Equation Solver (EES) yazılımı kullanılarak yapılmıştır.

Anahtar Kelimeler: Önleme Sistemi, Çoklu nesil Sistemi, Enerji, Ekserji, Verimlilik.

ACKNOWLEDGMENT

First and foremost, I would like to thank my supervisor and director of EMU energy research center Prof. Dr. Uğur Atikol for giving me the opportunity to work on this project and for the support of my master's research.

I would like to thank Asst. Prof. Dr. Tahir Abdul Hussain Ratlamwala who helped me with the project.

Special thanks go to my brother Gholamali Sharifisourabi, a postdoctoral fellowship in Canada, for his help and support. Also, I owe my deepest gratitude to my father, my sisters and my other brothers (Gholamreza, Mohammad Kazem, and Mohsen) for various the kind of assistance they have offered me.

Finally, I would like to thank all the members and employees of Mechanical Engineering Department at Eastern Mediterranean University for their everlasting support.

TABLE OF CONTENTS

LIST OF TABLES

LIST OF FIGURES

LIST OF SYMBOLS AND ABBREVIATIONS

ABS	Absorber
CH	Condensing Heat Exchanger
CO1	Condenser1
CO2	Condenser2
COP	Coefficient of Performance
d	Destruction
DEAS	Double Effect Absorption System
ELE	Electrolyzer
En	Energy
EVA	Evaporator
Ex	Exergy
EX1	Expansion Valve1
EX2	Expansion Valve2
h	Enthalpy
HST	Hydrogen Storage Tank
HTG	High Temperature Generator
HTH	High Temperature Heat Exchanger
HPG	High Pressure Generator
LPG	Low Pressure Generator
LTG	Low Temperature Generator
LTH	Low Temperature Heat Exchanger
MPG	Medium Pressure Generator
MTG	Medium Temperature Generator

MTH	Medium Temperature Heat Exchanger
$\dot{m}$	Mass flow rate
ORC	Organic Rankine Cycle
P	Pressure
P1	Pump1
P2	Pump2
PTSC	Parabolic Trough Solar Collector
$\dot{Q}$	Heat transfer rate
s	Entropy
SEAS	Single Effect Absorption System
SG	Steam Generator
T	Turbine
t	Temperature
TEAS	Triple Effect Absorption System
η	Energy Efficiency
ψ	Exergy Efficiency
ε	Utilization factor

Chapter 1

INTRODUCTION

1.1 Importance of Energy

Energy has an important role to play in the development of countries and by developing new technologies which make our lives easier, and thus has become more important to us as a community to utilize and develop alternative sources of energy. Consequently, adequate and authentic energy resources are essential for economic development of countries.

Pursuant to the data given by the International Energy Agency [1], the population of the world is predicted to grow at the rate of 5.6% whereas the consumption of energy is projected to rise at the rate of 9.2%. Between 2010 and 2015 humanity depended deeply on fossil fuels, such as gas, coal, and oil that offered nearly 80% of the universal energy needs to supply its energy requests. Fossil fuels and partial natural sources which are necessarily consumed were destroyed [2].

Moreover, global environmental issues and energy challenges have pushed many countries to create incentives, initiatives and methods to increase renewable energy resources and minimize or replace the use of fossil fuels [3, 4]. Since fossil fuels currently release toxic pollutants the creation and utilization of alternative energy sources such as solar, geothermal, wind energy, hydropower and nuclear energy are essential [5,6]. Solar energy has been surveyed to be one of the top alternative energy

sources since it is a free and renewable energy source that does not transmit any toxic gas emissions [7].

Due to the benefits of solar energy, the number of power plants being operated by solar energy has largely increased in recent times. Various solar thermal systems such as solar towers, solar dishes and Parabolic Trough Solar Collectors (PTSCs) can be used to generate power. The Parabolic Trough Solar Collectors are the most frequently used solar technology when using solar energy as a source of power [8].

1.2 Motivation

Energy is a vital portion of the world. Fossil fuels are the main energy resources which are being utilized in our daily activity and over-consumption can lead to serious problems such as environmental hazards, acid rain, and effect on human health.

Using energy resources efficiently is a major solution which results in beneficial productions, as well as positive environmental and economic impact. Multi-Generational systems have an interesting role in this regard. Multi-generational systems, which can generate several products at a time are far more efficient and more effective than systems that can only produce one product at a time.

These proposed systems will primarily be used in the residential sector, for establishments such as hotels. In this system, a solar power plant is integrated with a Triple Effect Absorption System (TEAS) and an electrolyser to produce heat, hot water, cooling, electricity, dry air and hydrogen. This is especially significant since hydrogen proves to be an environmentally-friendly element with no pollutant discharge which can be saved and used in future.

1.3 Objectives

The current study attempts to simulate the performance of a multi-generational system. Exergetic and energetic approaches will now be used to study and analyze the new multi-generational systems in detail. The exergy destructions are calculated for all major components. Moreover, the energetic and exegetic efficiency of Organic Rankine Cycle and also energetic and exegetic COP of absorption chiller are determined. The parametric studies will be undertaken in order to investigate the effects of varying state properties that surround the operating conditions.

1.4 Organization of the Thesis

The organization of the present research is stated as follows:

- Chapter 2 contains a review of the history of energy and exergy analyses.
- Chapter 3 contains the thermodynamic analysis which is beneficial for exergy and energy analyses.
- The description of the system is reported in chapter 4.
- The results of energy and exergy analyses of the system are presented in chapter 5.
- Moreover, in chapter 6 the conclusions are made.

Chapter 2

LITERATURE REVIEW

The value of solar energy which reaches the upper atmosphere of earth is around $1{,}350\mathrm{W/m^2}$. The atmosphere absorbs and scatters some of the energy [9]. The value of the energy of sun reaching the earth's surface also relies on location, air pollution, cloud cover and the period of time. An active solar process uses mechanical tools to gather, collect and distribute the sun's heat. An active process is made of a storage medium, a distribution system, and solar collectors. The active solar process is usually used for Solar/mechanical energy, space conditioning heat processing, electricity production, and water heating. Concentrated solar collectors are applied once higher temperatures are needed. Solar energy can be concentrated from reflective surfaces occupying large areas lines or points for obtaining more energy or heat. The part which absorbs the concentrated energy is smaller than the part taking the energy and consequently, reaches a high temperature before heat loss due to convection wastes and radiation of the energy which has been collected [10].

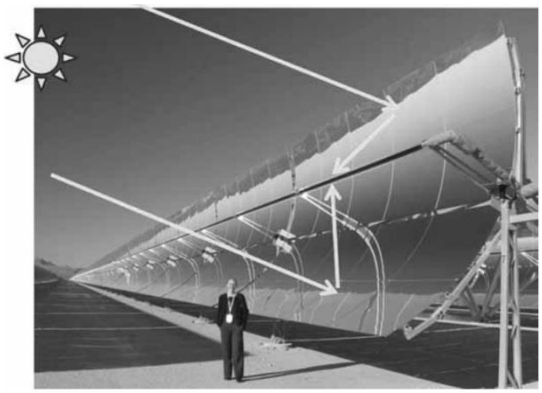

Figure 2.1. Schematic of a parabolic trough collector as presented in ref. [11]

In order to concentrate sunlight to a solar tubular receiver, a parabolic trough reflector system uses linear parabolic concentrators located along their focal line. Parabolic solar trough systems are typically ranged by their lengthy axes from north to south. Along the focal line, there is a fluid that absorbs the solar energy. The maximum fluid heat transfer temperature does not exceed 450°C, which is not sufficient to transmit heat to all parts in a Thermo-chemical system.

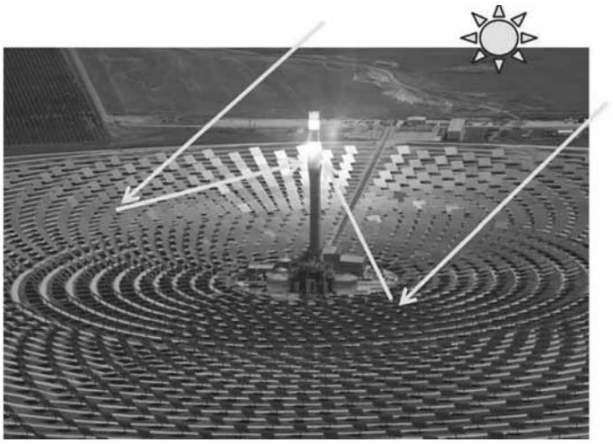

Figure 2.2. Schematic of a central receiver as presented in ref. [11]

Heliostat solar tower has the significant advantage of getting great production capabilities in a single part which focuses the reflections. The heat transfer fluid temperature can have a maximum temperature of 1000°C.

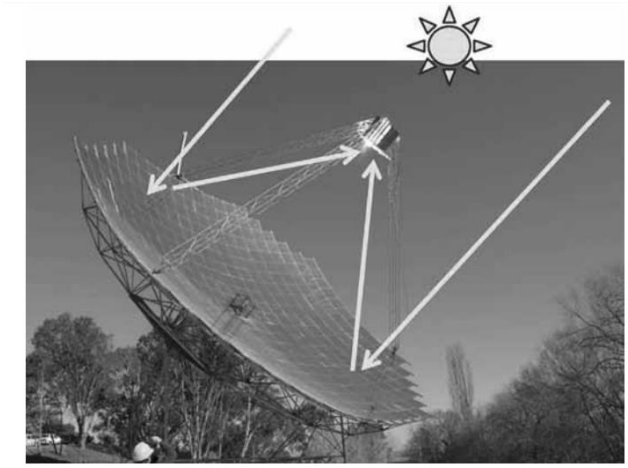

Figure 2.3. Schematic of a parabolic dish as presented in ref. [11]

In the parabolic dish systems, the point focus collectors normally follow and track the sunlight along two directions. They concentrate the insulation onto the receivers placed at the focal points, thus, It is possible to achieve temperatures of 1500°C. The double concentration systems usually consist of reflective towers, heliostat fields and ground receivers which are attached to the secondary concentrators.

It was shown by Delisle and Kummert [12] that PV systems produce more equivalent useful energy compared to the PV/T systems. For example, for a water temperature of 10°C at the inlet of the heat exchanger, the PV system produces 5 to 29 percent more equivalent useful energy compared to the PV/T system. Optical efficiency obtained from the theoretical optical efficiency is 71% while from the thermal measurement it is maximum efficiency is 65%.

This discrepancy is due to the thermal losses caused by reflector imperfections and by the photo voltaic-thermal absorber. The concentrating collectors are mostly only able to concentrate the parallel insulation which comes straight from the sun disk and therefore should follow and track the sun's path in the sky. Three kinds of solar concentrators are most common; central receivers, parabolic troughs, and parabolic dishes. These concepts are schematically shown in Figures 2.1-2.3.

The reactor/receiver on the earth can get temperatures higher than 1300°C [13-14]. It is possible to use different types of heat transfer fluid with these solar systems such as molten salt, air, and water. Among them, molten salt is more common because of its excellent advantage in storing solar energy for longer periods of time (i.e tens of hours) and then releasing it during the night hours [13].

2.1 Applications of PTSC

The parabolic trough solar collectors are being used in different fields. Their most popular applications are presented below.

2.1.1 Solar Power Generation

Because of the global warming issue and increased level of emissions, solar thermal energy is being increasingly applied.

There are two methods to integrate the PTSCs with solar thermal power. The first method is the DSG technology which includes using the steam generated by PTSCs to drive the steam turbine. In the second method, the solar thermal energy is used for heating a heat transfer fluid to be used in the heat exchanger to generate steam for running the steam turbine. However, both methods enable employing the PTSCs to drive all types of steam turbine power plants such as Organic Rankine Cycle, Rankine with regeneration, Rankine with superheat and Rankine with reheat [15].

2.1.2 Solar Refrigeration

Along with the rapid growth in refrigerated food consumption, the energy consumption of food processing industries has significantly increased as a large amount of energy is used for refrigerating the foods. Therefore, powering the refrigeration system with solar energy has recently attracted much attention of researchers and industries. There are different options that enable the integration of PTSC with a refrigeration system. For example, the PTSC can be used to power the absorption units.

2.1.3 Solar Desalination

Solar energy can also be used for water desalination. The water desalination systems consume huge amounts of energy. It is estimated that about 230 million tons of oil

per day is required for desalination of 25 million m3 of salty water per day. Therefore it is a good idea to use parabolic trough technology for desalinating the sea water as it is available in many regions. There are two systems used for water desalination which includes direct and indirect collection systems [16].

The first system directly uses the PTSC for desalination of salt water. In this system, the salt and water are separated by pumping the salt water through some troughs. In the second system, two sub-systems are needed; one of them is for energy collection and the other one is for desalination. A heat transfer fluid flows into the PTSC which supplies the heat demand for a steam boiler after which salt water is pumped into it and then condensed to generate freshwater [17].

2.2 Overall Heat Engine Systems

Heat engine cycles normally create power. The fundamental thermodynamic law includes a low temperature heat sink and a high temperature heat source. By concerning these sinks, a heat engine system converts a part of the heat stream to shaft work which is employed to generate power. Normally, in big measure processes high temperature heat resources from natural gas, coal, nuclear power and fuel oil and heat systems are identified as a Rankine Cycle. The advantage of Rankine cycles is that their return work ratio is much smaller than the return work ratio in the Brayton cycle [18].

A fluid, usually water, is circulated in the Rankine Cycle and the temperature is raised up to a superheated vapor state with high pressure. Then, it follows a path as it expands along a turbine which drops the temperature and pressure of the fluid whilst taking work from it. The exiting fluid is chilled to a saturated liquid after which it is

then pumped to the heat resource in order to vaporize the fluid. Several developments to such system are done to increase the efficiency and decrease the destruction which has affected it over time. The efficiencies of turbines have developed to achieve more energy from its fluid. To improve overall efficiency, other developments such as joining a gas turbine cycle to Rankine cycle are done too.

Low temperature resources such as industrial heat waste and solar are areas which utilize different types of Rankine cycle. Organic Rankine Cycle is similar to the Rankine cycle excluding the working fluid which typically is not water.

An organic cycle as a typical Rankine cycle has some components such as turbine, boiler pump, and condenser. The working fluid attracts heat in the boiler and then expands to a superheated vapor in the turbine. When it exits from the turbine, the temperature of the working fluid drops and transforms into a saturated liquid in the condenser. In order to increase the pressure into a circulating working fluid, a pump is available, Several structures for an ORC are available. The structure which is presented above is like a conventional Rankine cycle in the aspect of the components which is required for the process. There are some more typical structures such as combined heat and power organic Rankine cycle and regenerative organic Rankine cycle.

Combined Heat and Power Organic Rankine Cycles is like a basic ORC but after the turbine, there is a heat exchanger to take benefit of the rest of the heat which still may be at a high adequate temperature for practical usage.

2.3 Type of Absorption Chiller

Absorption chillers are usually categorized as single, double or triple effect and as direct or indirect-fired. In the direct-fired system, the heat resource can be the fuel which can be burnt in the systems such as gas. Indirect-fired systems use steam and some others transfer fluid which takes heat from a separate source like a boiler. Hybrid systems, that are fairly common with absorption chillers, combine electric process and gas process for load flexibility and optimization [19].

Figure 2.4 shows a schematic of a single effect absorption system. The single effect absorption chiller expresses the fluids transmission through the main sub-unites such as absorber, evaporator, condenser, and generator.

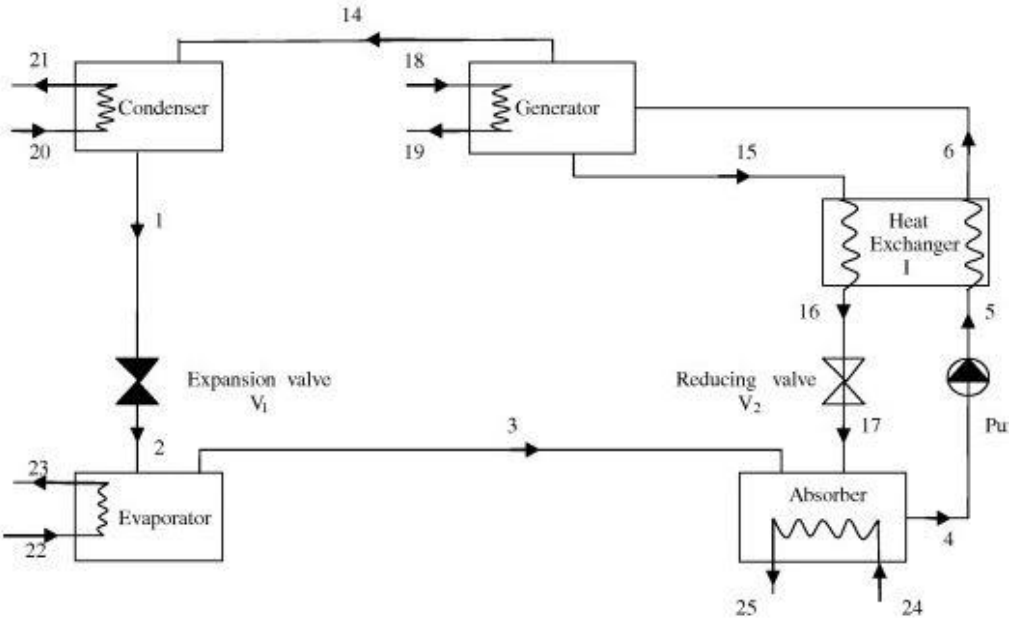

Figure 2.4. Schematic of a single effect absorption system as presented in ref. [20]

Single effect LiBr-water absorption system uses steam in low pressure or hot water as its heat source. The water is capable of evaporating and taking the heat in the evaporator since the chiller is under a partial vacuum. single-effect absorption

systems have a low thermal efficiency. Single-effect absorption system can be used to generate cool water and cooling process for air-conditioning.

The need for higher efficiency absorption chillers led to the development of a double-effect LiBr-water system. There are some differences between the double-effect absorption system and single-effect. The single effect absorption system has one generator while the double effect absorption chiller has two generators to gain more efficient production.

A Schematic of a double effect absorption cycle is illustrated in figure 2.5. The high pressure generator (HPG) uses the steam which is provided from outside to boil the refrigerant. The vapor from the low Pressure generator is going to condense by the condenser and then it goes to the evaporator.

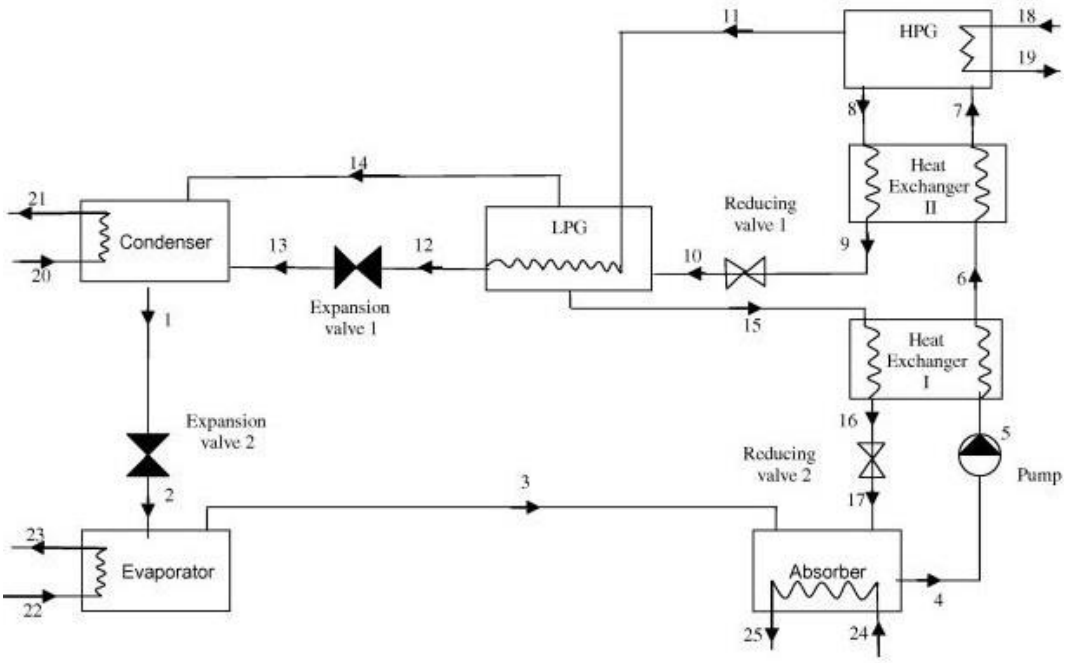

Figure 2.5. Schematic of a double effect absorption system as presented in ref. [20]

Double effect absorption systems use high pressure steam or gas-fired combustors as its heat source. Double effect absorption system can be used for process cooling and air-conditioning in areas where the electricity cost is higher than natural gas. Double-effect absorption systems can also be used in sectors where steam with high pressure is easily available. Moreover, the efficiency of the double effect systems is higher than single effect systems.

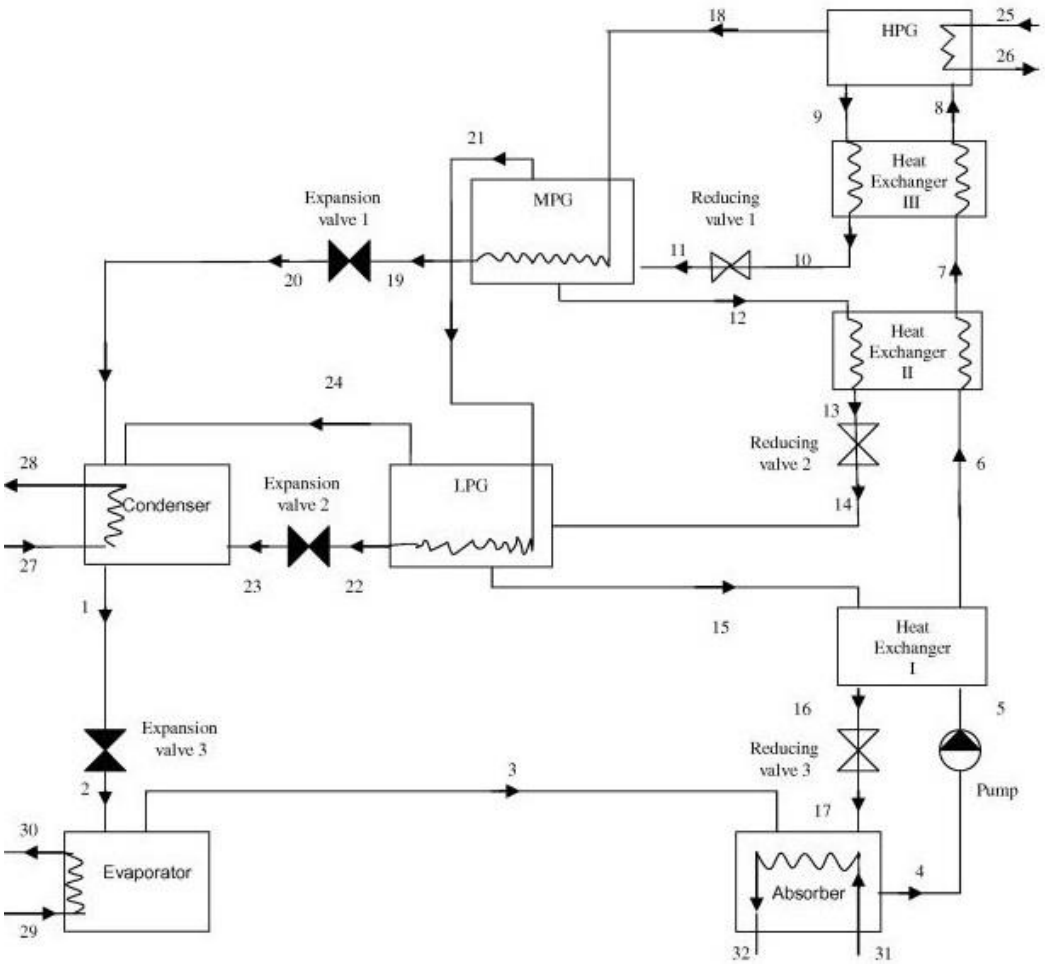

Figure 2.6. Schematic of a triple effect absorption system as presented in ref. [20]

The triple effect absorption systems are the next advancement after the double effect absorption systems. A Schematic of a triple effect absorption chiller is shown in figure 2.6. The refrigerant vapor is extracted from the high pressure generators and

then passed through the medium pressure generator and low pressure generator. The evaporator receives refrigerant of the condenser to absorb heat.

Al-Sulaiman et al. [21] conducted the exergy modeling of the trigeneration process based on solar. They considered three operation modes; solar mode and storage mode. They found that the highest electrical exergy efficiency of the solar and storage mode was 3.5%, solar mode was 7% and storage mode was3%. It was also discovered that by using the tri-generation system, the energy efficiency increases drastically. The maximum exergy efficiency of tri-generation for solar and storage mode was 8%, with the solar mode being 20% and the storage mode being 7%.

Ratlamwala et al. [22] proposed a combined triple effect absorption cooling system and proton exchange membrane (PEM) fuel cell. Their results showed that by increasing the fuel cell operating temperature, the fuel cell efficiency raised from 40% to 44.5%. Nevertheless, by increasing the temperature of the fuel cell, the energy production of the fuel cell ranged from 7.4kW to 10.7 kW and so, the COP reduced from 2.4 to 0.9. Moreover, they found that by the rise in both membrane thickness and density of fuel cell the fuel cell efficiency reduced from 41% to 32%. Also by the rise in the molar flow rate and density, the total utilization factor of their system declined from 84% to 35%.

In another research, Ratlamwala et al. [23] proposed a new system based on geothermal integration with double flash power generation, quadruple effect absorption cooling system and electrolyzer system for hot water, heating, cooling, electricity, and hydrogen production. It was found that increasing the temperature mass flow rate and pressure of the geothermal source, caused increased power and

hydrogen production rate. The hydrogen produced increased from 1.85 kg/day to 11.67 kg/day with an increase in temperature of the geothermal source from 440 K to 500 K respectively, and also, it increased from 7.9 kg/day to 9.6 kg/day by a rise in pressure of geothermal source from 3000 (kPa) to 5000 (kPa), respectively. Nevertheless, the rise in geothermal source pressure mass flow rate and temperature had negative effects on cooling generation.

Ozturk and Dincer [24] proposed a new multi-generation system based on solar to generate power, cooling, heating, hot water, oxygen, and hydrogen. They found that the exergy efficiency of their system was 57.35% and the energy efficiency of their system was 52.71%.

Ratlamwala, T. A. H., and I. Dincer developed and studied an integrated system based on geothermal containing quadruple effect absorption cooling system (QEACS), quadruple flash power plant (QFPP), airconditioning process and electrolyzer which was capable of providing heating, hot water, power, cooling, dry air and hydrogen as products. They found that with increase in geothermal liquid temperature from 450 K to 500 K and the increase in number of generations from single to hextuple generation, the exergy efficiency increased from 0.20 to 0.28 [25].

Murat and Dincer, developed a multi-generation system based on renewable energy involving power, cooling, heating, oxygen, hydrogen, hot water and coal gasification. Their results showed that energetic and exergetic COP of the SEAS were determined as 0.7587 and 0.3473, respectively [26].

Ahmadi et al. [27] developed a new multi-generation system for domestic uses, such as cooling, heating, hot water, electricity generation and hydrogen production through exergy analysis. They found that the multi-generation can increase the energy efficiency of the cycle by about 60% where before was double the exergy efficiency.

Ahmadi et al. [28] tested a system in which an ocean thermal energy conversion was accomplished by using PV/T solar collectors and a flat plate. Their studies showed that the multi-objective optimization exergy efficiency of 60% was the most beneficial.

Zamfirescu and Dincer [29] developed and analyzed a novel system in order to produce hydrogen which was integrated with a heat engine, photocatalytic reactor and photovoltaic. They found that the annual average improvement factor of light absorption with a new system was 10%. In addition, the overall exergy efficiency of hydrogen generation increased by 40%. Moreover, the average exergy efficiency of hydrogen generation was 20%.

Yusuf and Dincer have designed and analyzed an integrated system for syngas, bitumen, electricity and hydrogen production at the same time with steam assisted gravity drainage and underground coal gasification (UCG). The proposed system highlights the significance of multi-generation systems. In their study, energy efficiencies of components were determined as 75% for UCG process and 50% for Brayton cycle. Exergy and energy efficiencies of the overall system were 17.3% and 19.6%, respectively [30].

Khalid et al. have developed a new renewable system based on multi-generation through energy and exergy analysis. The overall exergy and energy efficiencies of the proposed system, which uses solar energy and biomass were 39.7% and 66.5% respectively. On the other hand, the exergy and energy efficiencies were 37.6% and 64.5% respectively when the system operated with only biomass while the exergy and energy efficiencies were 44.3% and 27.3% when the system operated with only solar [5].

Islam et al. performed comprehensive exergy and energy analysis of a novel multigeneration system based on solar containing thermoelectric generators. The exergy and energy efficiencies of PV panels without thermoelectric generators were determined to be 5.9% and 5.6%, respectively, while with thermoelectric generators exergy and energy efficiencies were calculated to be 10.7% and 10.1% respectively. The exergy and energy efficiencies of single generation cycle without thermoelectric devices were determined to be 33.2% and 16.7% whereas with thermoelectric generators, exergy and energy efficiencies were calculated to be 33% and 16.7%, respectively. The exergy and energy efficiencies of overall system without thermoelectric generators were determined to be39.8% and 50.6% respectively While with thermoelectric generators exergy and energy efficiencies were calculated to be 40.32% and 51.33%, respectively [31].

Yusuf and Dincer designed a novel multi-generation system with hydrogen production. For 20 kg/s coal feed rate, the highest exergy and energy efficiencies were determined to be 26% and 29.2%, respectively. They found that the Heat Exchanger 1, gas turbine and water tank and treatment have high exergy destruction

rates as a sub-system accounting for almost 60% of the overall exergy destruction rates of the whole system [32].

Malik et al. [33] developed and analyzed a new multi-generation system through energy and exergy. The overall exergy and energy efficiencies of the system were found to be 20.3% and 56.5% respectively. Also, the exergy and energy efficiencies of the ORC were given as 42.3% and 52.2% respectively. Moreover, the exergetic and energetic COP of the absorption chiller system were found to be 0.13 and 0.69, respectively.

Furthermore, Al-Sulaiman et al. [34] analyzed a tri-generation system based on biomass integrated with an organic Rankine cycle (ORC) through energy and exergy. They found that the maximum exergy efficiency of the ORC was 13% and by using trigeneration it increased by 15% and reached up to 28%.

Chapter 3

SYSTEM DESCRIPTION

As shown in figure 3.2, the multi-generation system of this study, configuration and layout consists of five major subsystems:

1. Parabolic Trough Solar Collector (PTSC)
2. Organic Rankine Cycle (ORC)
3. Absorption chiller
4. Dryer
5. Electrolyzer

The main outputs of the given system are electricity, dry air, cooling, heating, hot water and hydrogen. Solar energy is employed as the energy source in this system. The thermal energy of the solar radiation is collected using a Parabolic Trough Collector which is made up of two sub-units: the heat engine unit and the collector–receiver unit. The collector–receiver circuit involves a few parabolic collectors prepared in units that drive in a tracking mode so that the working fluid can move within them.

In this system, solar collectors attract solar radiation and transfer it to passing the molten salt. The molten, 60NaNO3_40KNO3, takes heat and passes it through the Steam Generator to vaporize the Rankine organic fluid. This process runs the turbine.

The heat ejected from the ORC will also be transferred to the triple effect absorption system generator so that it runs the TEAS. LiBr-water and R134-a were selected as working fluids for TEAS and the dryer cycle respectively.(The Properties of the Molten Salt is demonstrated in Table 3.1)

Table 3.1. Properties of the Molten Salt

Type of the Molten Salt	NaCl-MgCl2
Freezing point (ºC)	445
Normal boiling point (ºC)	>1465
900ºC vapor pressure (mm Hg)	< 2.5
Melting Point (ºC)	450
Density (g/cm3)	1.677
Heat Capacity (cal/g-ºC)	0.262

The ORC is made up of four components: a pump, a steam generator, a turbine, and a condenser. The ORC working fluid must have a high temperature to ensure an efficient process. In this parametric study, n-octane was chosen as the working fluid. The n-octane has high thermal capabilities and is easily available. Therefore, using n-octane will allow for more heat to be transmitted from the solar system to the working fluid (Figure 3.1 and Table 3.2).

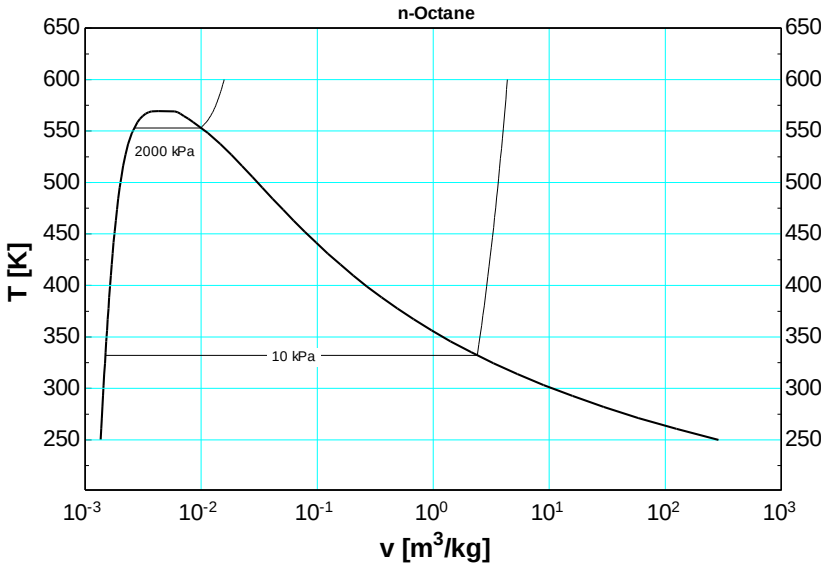

Figure 3.1 The T-v diagram of n-Octane

Heat from the Organic Rankine Cycle is provided to the High Temperature Generator (HTG) of the Triple Effect Absorption System to create cooling and hot water. The heat delivered is used in the HTG, in which at state 28 a weak solution is heated. A strong solution and water vapor are exited at states 29 and 30 respectively. At state 29, the strong solution transfers heat to state 25 in the High Temperature Heat exchanger (HTH). At state 32, it combines with the solution from state 12 and then transfers heat to the state 20 in the Medium Temperature Heat exchanger (MTH). The solution goes into the Low Temperature Heat exchanger (LTH) and transfers the heats to the solution going at state 19. The solution passing through the expansion valve, decreases its temperature and goes to the absorber. At state 30, the vapor goes in the Medium-Temperature Generator (MTG) and heats the solution at state 26 then exits as a vapor at states 27 and 4. At state 5, they combine and then go to the Low Temperature Generator (LTG), where it heats the weak solution at state 22 and then leaves at states 6 and 7 as a vapor. The fluid at state 7 enter the condenser and at state 6 enters the Condensing Heat exchanger(CH) and heats the fluid incoming at state 17 which leaves at state 18. The vapor exits the CH at state 8 and goes into the condenser, and exit at state 9. The flow goes into the expansion valve and at state 10 it goes into the evaporator. The evaporator receives the heat, exits at state 11 and goes into the absorber. All three flow mix in the absorber, release heat, and then it goes to the pump at state 1.

Table 3.2 properties of n-Octane

Chemical Name	n-Octane
Molecular Formula	C8H18
Melting Point (ºC)	-57
Boiling point(ºC)	125-127
Density g/mL at 25 °C	0.703

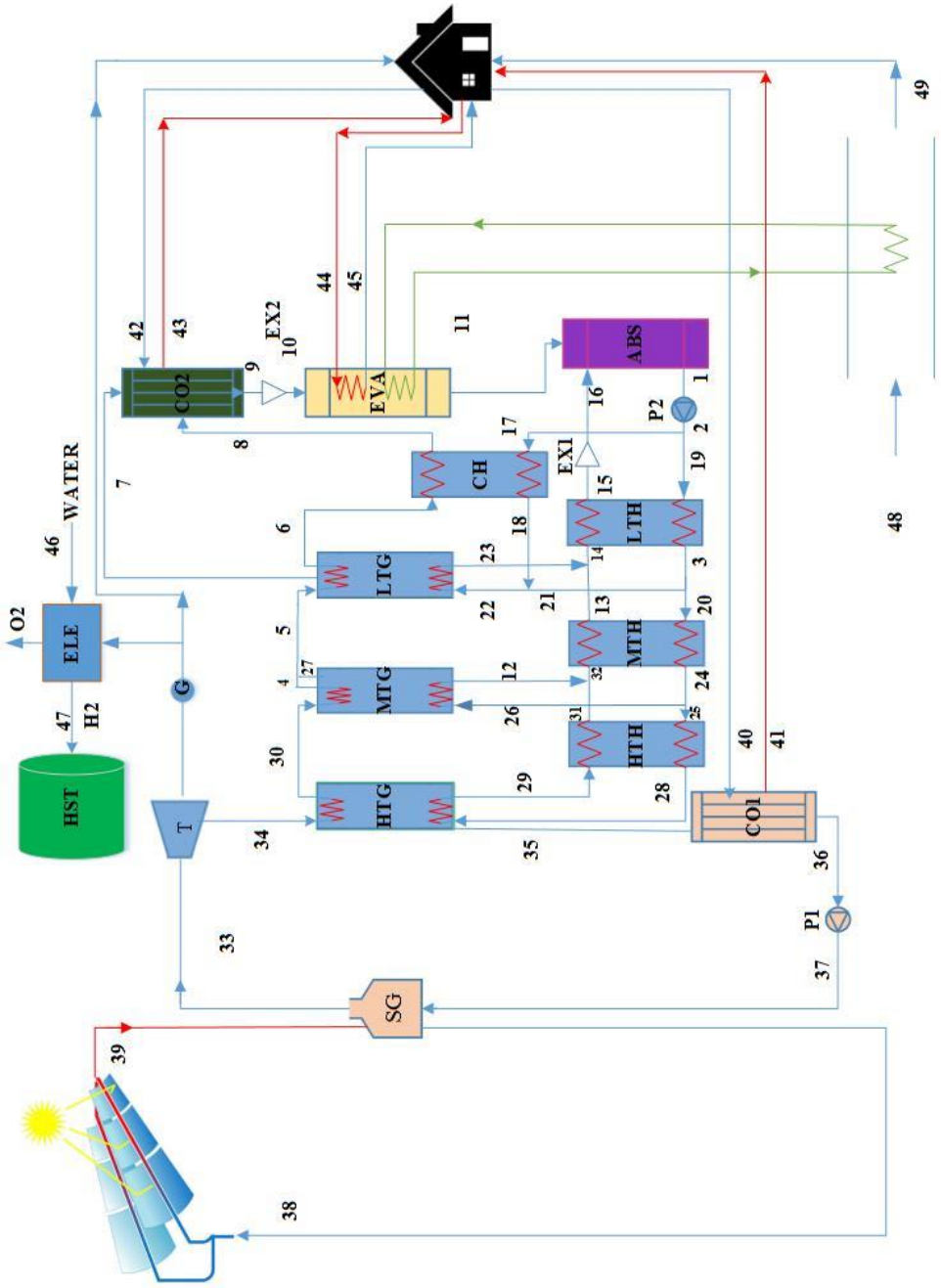

Figure 3.2. The schematic of proposed multigeneration system

Chapter 4

METHODOLOGY

Chapter 4 is prepared in the following arrangement: In the beginning, schematic of each component is represented and then mass, energy and exergy analysis are defined.

The following assumptions are made for the analysis of the system:

- Air is treated as an ideal gas.
- The reference environment state has a temperature of T[0] = 298 K and a pressure of P[0] = 100 kPa.
- The changes in potential and kinetic exergy and energy are negligible.
- The heat exchangers do not have any heat losses.
- The pressure losses in all pipelines and heat exchangers are negligible.

According to [35], the mass, energy and exergy balances for the major components can be written as follows:

4.1 Turbine (T)

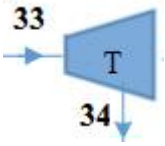

Figure 4.1. Schematic of Turbine

The mass, energy and exergy balance equations are written for Turbine:

Mass balance: $\dot{m}_{33} = \dot{m}_{34}$ (1)

Energy balance: $\dot{m}_{33} h_{33} = \dot{m}_{34} h_{34} + \dot{w}_T$ (2)

Exergy balance: $\dot{m}_{33} ex_{33} = \dot{m}_{34} ex_{34} + \dot{w}_T + \dot{E}x d_T$ (3)

4.2 Condenser 1 (CO1)

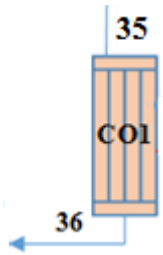

Figure 4.2. Schematic of Condenser1

The mass, energy and exergy balance equations for Condenser1 can be written as:

Mass balance: $\dot{m}_{35} = \dot{m}_{36}$ (4)

Energy balance: $\dot{m}_{35} h_{35} = \dot{m}_{36} h_{36} + \dot{Q}_{co1}$ (5)

Exergy balance: $\dot{m}_{35} ex_{35} = \dot{m}_{36} ex_{36} + \dot{Q}_{co1}(1 - \frac{T_0}{T_s}) + \dot{E}x d_{c1}$ (6)

4.3 Pump1 (P1)

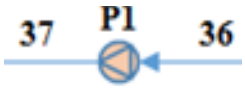

Figure 4.3. Schematic of Pump1

The mass, energy, exergy balance equations for pupm1 are provided below:

Mass balance: $\dot{m}_{36} = \dot{m}_{37}$ (7)

Energy balance: $\dot{w}_{p1} = \dot{m}_{36}(h_{36} - h_{37})$ (8)

Exergy balance: $\dot{m}_{36}\, ex_{36} + \dot{w}_{p1} = \dot{m}_{37}\, ex_{37} + \dot{E}x\, d_{P1}$ (9)

4.4 Steam Generator (SG)

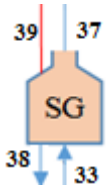

Figure 4.4. Schematic of Steam Generator

The balance equations for Steam Generator can be written as follow:

Mass balances: $\dot{m}_{38} = \dot{m}_{39}, \dot{m}_{33} = \dot{m}_{37}$ (10)

Energy balance: $\dot{m}_{38}\, h_{38} + \dot{Q}_{SG} = \dot{m}_{39}\, h_{39}$ (11)

Exergy balance: $\dot{m}_{39}\, ex_{39} + \dot{m}_{33}\, ex_{33} = \dot{m}_{38}\, ex_{38} + \dot{m}_{37}\, ex_{37} + \dot{E}x\, d_{SG}$ (12)

4.5 High Temperature Generator (HTG)

Figure 4.5. Schematic of High Temperature Generator

Mass balances: $\dot{m}_{34} = \dot{m}_{35}, \dot{m}_{28} = \dot{m}_{29} + \dot{m}_{30}$ (13)

Energy balance: $\dot{m}_{34}\, h_{34} = \dot{m}_{35}\, h_{35} + \dot{Q}_{HTG}$ (14)

Exergy balance: $\dot{m}_{34}\, ex_{34} + \dot{m}_{28}\, ex_{28} = \dot{m}_{35}\, ex_{35} + \dot{m}_{30}\, ex_{30} + \dot{m}_{29}\, ex_{29} + \dot{E}x\, d_{HTG}$ (15)

4.6 Medium Temperature Generator (MTG)

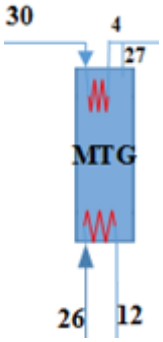

Figure 4.6. Schematic of Medium Temperature Generator

The mass, energy and exergy balance equations are written for MTG:

Mass balances: $\dot{m}_{26} = \dot{m}_{12} + \dot{m}_{27}, \dot{m}_{30} = \dot{m}_{4}$ (16)

Energy balance: $\dot{m}_{26}\, h_{26} + \dot{Q}_{MTG} = \dot{m}_{12}\, h_{12} + \dot{m}_{27}\, h_{27}$ (17)

Exergy balance: $\dot{m}_{26}\, ex_{26} + \dot{m}_{30}\, ex_{30} = \dot{m}_{4}\, ex_{4} + \dot{m}_{12}\, ex_{12} + \dot{m}_{27}\, ex_{27} + \dot{E}x\, d_{MTG}$ (18)

4.7 Low Temperature Generator (LTG)

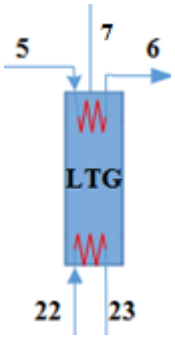

Figure 4.7. Schematic of Low Temperature Generator

The mass, energy and exergy balance equations for LTG are provided below:

Mass balances: $\dot{m}_{22} = \dot{m}_{23} + \dot{m}_{6}, \dot{m}_{5} = \dot{m}_{2}$ (19)

Energy balance: $\dot{m}_{22} h_{22} + \dot{Q}_{LTG} = \dot{m}_{23} h_{23} + \dot{m}_{6} h_{6}$ (20)

Exergy balance: $\dot{m}_{5} ex_{5} + \dot{m}_{22} ex_{22} = \dot{m}_{6} ex_{6} + \dot{m}_{7} ex_{7} + \dot{m}_{23} ex_{23} + \dot{E}x d_{LTG}$ (21)

4.8 High Temperature Heat Exchanger (HTH)

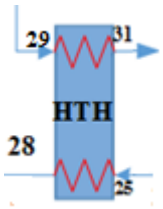

Figure 4.8. Schematic of High Temperature Heat Exchanger

The mass, energy and exergy balance equations for HTH are represented below:

Mass balances: $\dot{m}_{29} = \dot{m}_{31}, \dot{m}_{25} = \dot{m}_{28}$ (22)

Energy balance: $\dot{m}_{29} h_{29} = \dot{m}_{31} h_{31} + \dot{Q}_{HTH}$ (23)

Exergy balance: $\dot{m}_{25} ex_{25} + \dot{m}_{29} ex_{29} = \dot{m}_{28} ex_{28} + \dot{m}_{31} ex_{31} + \dot{E}x d_{HTH}$ (24)

4.9 Medium Temperature Heat Exchanger (MTH)

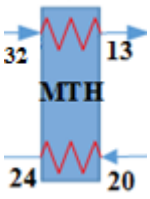

Figure 4.9. Schematic of Medium Temperature Heat Exchanger

The mass, energy and exergy balance equations for LTG are provided as follow:

Mass balances: $\dot{m}_{32} = \dot{m}_{13}, \dot{m}_{20} = \dot{m}_{24}$ (25)

Energy balance: $\dot{m}_{32} h_{32} = \dot{m}_{13} h_{13} + \dot{Q}_{MTH}$ (26)

Exergy balance: $\dot{m}_{32}\, ex_{32} + \dot{m}_{20}\, ex_{20} = \dot{m}_{13}\, ex_{13} + \dot{m}_{24}\, ex_{24} + \dot{E}x\, d_{MTH}$ (27)

4.10 Low Temperature Heat Exchanger (LTH)

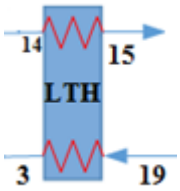

Figure 4.10. Schematic of Low Temperature Heat Exchanger

The balance equations for LTH can be written as follow:

Mass balances: $\dot{m}_{19} = \dot{m}_3, \dot{m}_{14} = \dot{m}_{15}$ (28)

Energy balance: $\dot{m}_3\, h_3 = \dot{m}_{19}\, h_{19} + \dot{Q}_{LTH}$ (29)

Exergy balance: $\dot{m}_{14}\, ex_{14} + \dot{m}_{19}\, ex_{19} = \dot{m}_{15}\, ex_{15} + \dot{m}_3\, ex_3 + \dot{E}x\, d_{LTH}$ (30)

4.11 Condensing Heat Exchanger (CH)

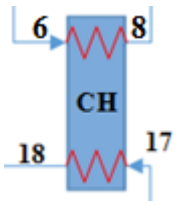

Figure 4.11. Schematic of Condenser Heat Exchanger

The balance equations for CH can be written as follow:

Mass balances: $\dot{m}_{17} = \dot{m}_{18}, \dot{m}_6 = \dot{m}_8$ (31)

Energy balance: $\dot{m}_{17}\, h_{17} + \dot{Q}_{CH} = \dot{m}_{18}\, h_{18}$ (32)

Exergy balance: $\dot{m}_6\, ex_6 + \dot{m}_{17}\, ex_{17} = \dot{m}_8\, ex_8 + \dot{m}_{18}\, ex_{18} + \dot{E}x\, d_{CH}$ (33)

4.12 Condenser 2 (CO2)

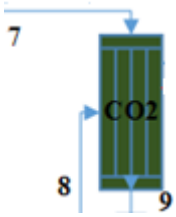

Figure 4.12. Schematic of Condenser 2

The mass, energy and exergy balance equations for CO2 are provided as follow:

Mass balance: $\dot{m}_7 + \dot{m}_8 = \dot{m}_9$ (34)

Energy balance: $\dot{m}_7 h_7 + \dot{m}_8 h_8 = \dot{m}_9 h_9 + \dot{Q}_{co2}$ (35)

Exergy balance: $\dot{m}_7 ex_7 + \dot{m}_8 ex_8 = \dot{m}_9 ex_9 + Q_c(1 - \frac{T_0}{T_{co2}}) + \dot{E}x d_{CO2}$ (36)

4.13 Pump 2 (P2)

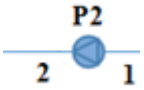

Figure 4.13. Schematic of Pump 2

The mass, energy and exergy balance equations for Pump2 are provided below:

Mass balance: $\dot{m}_1 = \dot{m}_2$ (37)

Energy balance: $\dot{w}_{p2} = \dot{m}_1(h_1 - h_2)$ (38)

Exergy balance: $\dot{m}_1 ex_1 + \dot{w}_{p2} = \dot{m}_2 ex_2 + \dot{E}x d_{P2}$ (39)

4.14 Evaporator (EVA)

Figure 4.14. Schematic of Evaporator

The mass, energy and exergy balance equations for EVA are provided as follow:

Mass balance: $\dot{m}_{10} = \dot{m}_{11}$ (40)

Energy balance: $\dot{m}_{10} h_{10} + \dot{Q}_{eva} = \dot{m}_{11} h_{11}$ (41)

Exergy balance: $\dot{m}_{10} ex_{10} + \dot{Q}_{eva}(1 - \frac{T_0}{T_{eva}}) = \dot{m}_{11} ex_{11}$ (42)

4.15 Absorber (ABS)

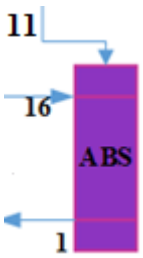

Figure 4.15. Schematic of Absorber

The balance equations for ABS can be defined as:

Mass balance: $\dot{m}_{11} + \dot{m}_{16} = \dot{m}_{1}$ (43)

Energy balance: $\dot{m}_{11} h_{11} + \dot{m}_{16} h_{16} = \dot{m}_{1} h_{1} + \dot{Q}_{abs}$ (44)

Exergy balance: $\dot{m}_{11}\, ex_{11} + \dot{m}_{16}\, ex_{16} = \dot{m}_{1}\, ex_{1} + \dot{Q}_{abs}\ \ (1-\frac{T_0}{T_{abs}}) + \dot{E}x\, d_{abs}$ (45)

4.16 Energetic and Exergetic COP of Absorption Chiller:

The energetic COP (COP_{En}) and exergetic COP (COP_{Ex}) of the absorption system can be determined from:

$$COP_{En} = \frac{\dot{Q}_{eva}}{\dot{Q}_{HTG} + \dot{w}_{Pump2}} \quad (46)$$

$$COP_{Ex} = \frac{\dot{EX}_{EVA}}{\dot{EX}_{HTG} + \dot{w}_{pump2}} \quad (47)$$

4.17 Energy and Exergy Efficiency of ORC

The energetic efficiency of ORC (η_{ORC}) and exergetic efficiency of ORC (Ψ_{ORC}) can be calculated from:

$$\eta_{ORC} = \frac{\dot{W}_{net}}{\dot{Q}_{SG}} \quad (48)$$

$$\Psi_{ORC} = \frac{\dot{W}_{net}}{\dot{EX}_{SG}} \quad (49)$$

4.18 Hydrogen Production Rate ($\dot{m}_{H_2}$)

$$\dot{m}_{H2} = \frac{\eta_{ELE} * \dot{W}_{ELE}}{HHV} \quad (50)$$

η_{ELE} is the efficiency of electrolyzer which supposed to be 0.56 and $\dot{w}_{ELE}$ is the work input for electrolyzer which its maximum can be equal to $\dot{w}_{net}$ and HHV is the high heating value of hydrogen which is equal to 141800 kJ/kg.

4.19 Drying Process

The equations for the drying process can be written as:

$$\dot{Q}_{Dryer} = \dot{m}_{48} * \mathrm{h}_{48} - (\dot{m}_{49} * \mathrm{h}_{49} + \dot{m}_{water} * h_{water}) \tag{51}$$

$$\eta_{Dryer} = \frac{\dot{m}_{49} * \mathrm{h}_{49}}{\dot{Q}_{Dryer}} \tag{52}$$

4.20 Turbine Efficiency

$$\eta_T = \frac{\dot{W}_T}{(\dot{m}[33] * h[33] - \dot{m}[34] * \mathrm{h}[34])} \tag{53}$$

4.21 Exergoenvironmental Analysis

$$\mathrm{f_{ei}} = \frac{\dot{\mathrm{E}}\mathrm{x}_{\mathrm{des,tot}}}{\dot{\mathrm{E}}_{\mathrm{x_{in}}}} \tag{54}$$

$$\mathrm{C_{ei}} = \frac{1}{\eta_{ex}/_{100}} \tag{55}$$

$$\theta_{\mathrm{ei}} = \mathrm{f_{ei}} \times \mathrm{C_{ei}} \tag{56}$$

$$\theta_{\mathrm{eii}} = \frac{1}{\theta_{\mathrm{ei}}} \tag{57}$$

$$\mathrm{f_{es}} = \frac{\dot{\mathrm{E}}\mathrm{x}_{\mathrm{tot,out}}}{\dot{\mathrm{E}}\mathrm{x}_{\mathrm{tot,out}} + \dot{\mathrm{E}}\mathrm{x}_{\mathrm{des,tot}}} \tag{58}$$

$$\theta_{\mathrm{est}} = \mathrm{f_{es}} \times \theta_{\mathrm{eii}} \tag{59}$$

Where $\dot{\mathrm{E}}\mathrm{x}_{\mathrm{des,tot}}$ is total exergy destruction rate, $\dot{\mathrm{E}}_{\mathrm{x_{in}}}$ is input exergy rate, η_{ex} represents exergy efficiency of the system, $\mathrm{f_{ei}}$ shows exergoenvironmental impact factor, $\mathrm{C_{ei}}$ is exergoenvironmental impact coefficient, θ_{ei} is exergoenvironmental impact index, θ_{eii} represents exergoenvironmental impact improvement, $\mathrm{f_{es}}$ is the exergy stability factor, and θ_{est} represents exergetic sustainability index.

Chapter 5

RESULTS AND DISCUSSION

In this thesis, a new system based on multi-generation is proposed, and energy and exergy analysis of all sub-system are determined. The study leads to the evaluation of the effects of changes in the environmental temperature on COP absorption chiller and the exergy destructions of major systems. All modeling and thermodynamic analysis have been done by Engineering Equation Solver (EES) software which included the calculation of properties such as enthalpy and entropy which are determined by using pressure and temperature of each state points. A comparative research was prepared and the results were found to be similar. To certify the simulation model, Some results are compared with a system which has been examined by Ahmadi et al.[4].

Table 5.1. Comparison of current study results with the results of Ahmadi et al.[4]

Quantity	Current study	Ahmadi et al.[4]
$\dot{Q}_{in}$ $[kW]$	2434.67	2434.67
η_{ORC} [%]	22	15
ψ_{ORC} [%]	35	24

Table 5.1 illustrates some comparison of results between this study and a previous study. Ahmadi et al.[4], proposed and assessed a new system based on multi-generation integrated with an organic Rankine cycle (ORC), a biomass combustor, a

proton exchange membrane electrolyser, a domestic water heater and an absorption chiller. As it is shown in table 1, by considering the same amount of heat injection to the system, the ORC exergy efficiencies obtained was (35%) and the energy efficiency of the ORC was found to be 22% for the current study which was slightly more comparable to their study which was around 15 % and 22 % respectively. The description of each state point is presented in table 5.2.

Table 5.2. Description of each state point

Point	Description	Point	Description
1	Weak solution entering pump	26	Weak solution entering MTG
2	Weak solution exiting pump	27	Water vapor exiting MTG
3	Weak solution exiting LTH	28	Weak solution entering HTG
4	Water vapor exiting MTG	29	Strong solution entering HTH
5	Mixing water vapor 4 and 27	30	Water vapor exiting HTG
6	Water vapor entering CH	31	Strong solution exiting HTH
7	Water vapor exiting LTG	32	Strong solution entering MTH
8	Water vapor entering condenser2	33	ORC working fluid entering turbine
9	Water entering expansion valve	34	ORC working fluid entering HTG
10	Water entering evaporator	35	ORC working fluid entering condenser1
11	Water entering absorber	36	ORC working fluid entering pump1
12	Strong solution exiting MTG	37	ORC working fluid entering SG
13	Strong solution exiting MTH	38	Molten salt entering PTSC
14	Strong solution entering LTH	39	Molten salt exiting PTSC
15	Strong solution entering expansion valve	40	Cold water entering condenser1
16	Strong solution entering absorber	41	Hot water exiting condenser1
17	Weak solution entering CH	42	Cold water entering condenser2
18	Weak solution exiting CH	43	Hot water exiting condenser2
19	Weak solution entering LTH	44	Hot water entering evaporator
20	Weak solution entering MTH	45	Cold water exiting evaporator
21	Weak solution adding to point 18	46	Water entering electrolyzer
22	Weak solution entering LTG	47	Hydrogen exiting electrolyzer
23	Weak solution exiting LTG	48	Humid air entering dryer
24	Weak solution exiting MTH	49	Dry air exiting dryer
25	Weak solution entering HTH		

Properties of different points are determined, such as temperature, pressure, mass flow rate, specific enthalpy, specific entropy and exergy rate as arranged in table 5.3.

Table 5.3. Properties at each state point in the current System

point	**t (K)**	**P (kPa)**	(kg/s)	h (kJ/kg)	S (kJ/kg.K)	Exergy rate (kW)
1	283.2	0.75	2.4	25.07	0.05775	3922
2	283.2	2.2	2.4	25.07	0.05775	3922
3	312.9	2.2	2.16	86.16	0.2628	3530
4	364.4	2.2	0.5861	2671	9.103	929
5	364.2	2.2	0.6056	2671	9.102	959.8
6	312.7	2.2	0.6056	2574	8.815	952.8
7	299	2.2	0.114	2548	8.731	179.3
8	292.2	2.2	0.6056	2509	8.687	936.8
9	275.9	2.2	0.7196	-88.44	0.0421	1098
10	275.9	0.75	0.7196	-88.44	0.0421	1098
11	280.1	0.75	0.7196	2513	9.107	1026
12	348.3	2.2	0.175	172.5	0.448	291.4
13	309.3	2.2	1.338	94.38	0.2101	2219
14	319.1	2.2	1.68	113.8	0.2721	2788
15	279.6	2.2	1.68	38.2	0.01923	2788
16	279.6	0.75	1.68	38.2	0.01923	2788
17	283.2	2.2	0.24	25.07	0.05775	392.2
18	360	2.2	0.24	187.7	0.564	395
19	283.2	2.2	2.16	25.05	0.05768	3530
20	312.9	2.2	1.944	86.16	0.2628	3177
21	312.9	2.2	0.216	86.16	0.2628	353
22	337.7	2.2	0.456	139.1	0.4254	747.2
23	357.7	2.2	0.342	191.6	0.502	570.6
24	328.3	2.2	1.944	118.9	0.3651	3181
25	328.3	2.2	1.75	118.9	0.3651	2863
26	328.3	2.2	0.1944	118.9	0.3651	318.1
27	358.3	2.2	0.01944	2660	9.071	30.77
28	349.7	2.2	1.75	165.2	0.5012	2873
29	365	2.2	1.163	206.7	0.5437	1944
30	417.2	2.2	0.5861	2772	9.36	942.9
31	331	2.2	1.163	137.5	0.3452	1933
32	333.3	2.2	1.338	142	0.3588	2224
33	707.3	2000	2.223	1352	2.732	4812
34	635.9	10	2.223	1160	2.82	4326
35	347.9	10	2.223	451.1	1.369	3711
36	313	10	2.223	33.38	0.1098	3617
37	313	2000	2.223	35.22	0.1064	3623
38	720	101.3	10	282	0.4529	17734
39	850	101.3	10	481.7	0.7079	18971
40	293	101.3	5	83.3	0.294	8110
41	337.4	101.3	5	269	0.8842	8159
42	293	101.3	20	83.3	0.294	32441
43	315.4	101.3	20	177	0.6022	32478
44	298	101.3	15	167	0.5702	19481
45	277.3	101.3	15	53.91	0.1925	19475
46	298	101	1	104.2	0.3648	1622
47	299	101	0.001662	-2.152	64.77	-29.38
48	308	101	5.397	128.4	5.764	200.9
49	288	101	5.397	41.69	5.759	-289.6

5.1 Effect of Ambient Temperature on the Net Work and Hydrogen Production

The effect of changing the inlet temperature of the turbine on the net work produced by turbine and hydrogen production is shown in figure 5.1. When the inlet temperature of turbine increases from 650 K to 750 K, both turbine net work and hydrogen production is grows. This is because by increasing turbine inlet temperature the inlet enthalpy increases and so the net work of turbine rising causes the increase in the amount of hydrogen been produced. It has been shown that increasing the mass flow has a direct effect on the net work of turbine and causes the increase in both turbine net work and amount of hydrogen production at a temperature of 650 K which resulted in the turbine net work of 339kW, 420.9kWand 442.5kW for an ORC mass flow rate of 2.223 kg/s ,2.3kg/s and 2.4 kg/s respectively. Also at temperature of 650 K the mass of hydrogen production are 0.0015 kg/s, 0.0016 kg/s and 0.0017 +kg/s for an ORC mass flow rate of 2.223 kg/s, 2.3kg/s and 2.4 kg/s, respectively.

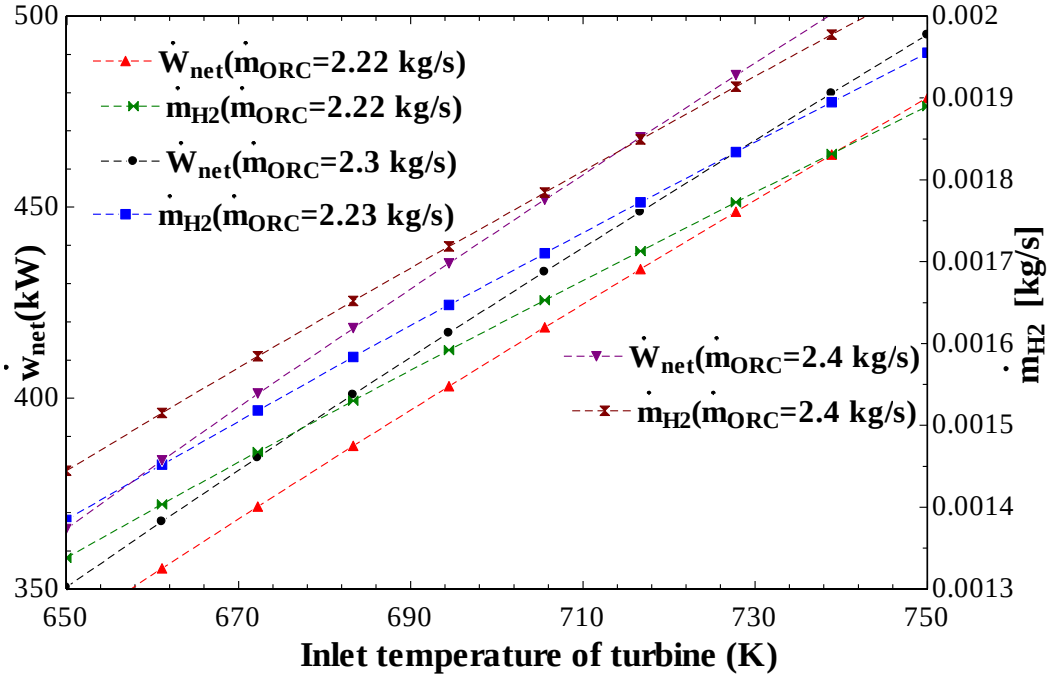

Figure 5.1. Effect of inlet temperature of turbine on the net work ($\dot{W}_{net}$) and hydrogen production ($\dot{m}_{H2}$)

5.2 Effect of Turbine Inlet Temperature on ORC Efficiencies

The effect of changing the turbine inlet temperature on the energy and exergy efficiency of the ORC is shown in Figure 5.2. It can be understood that by increasing the inlet temperature of turbine both energy and exergy efficiency of Organic Rankine Cycle increases but exergy efficiency has a slight increase in slope. These lines are linear because the heat input is supposed to be constant. In addition, it is clear that by increasing the inlet temperature of turbine the Carnot efficiency is increased. Moreover, It is illustrated that when the turbine inlet temperature increases from 650 (K) to 750 (K) the ORC energy efficiency grows from 16.97% to 23.97% and the ORC exergy efficiency increases from 27.35% to 38.63%. This is because of growth in the amount of inlet exergies and enthalpies.

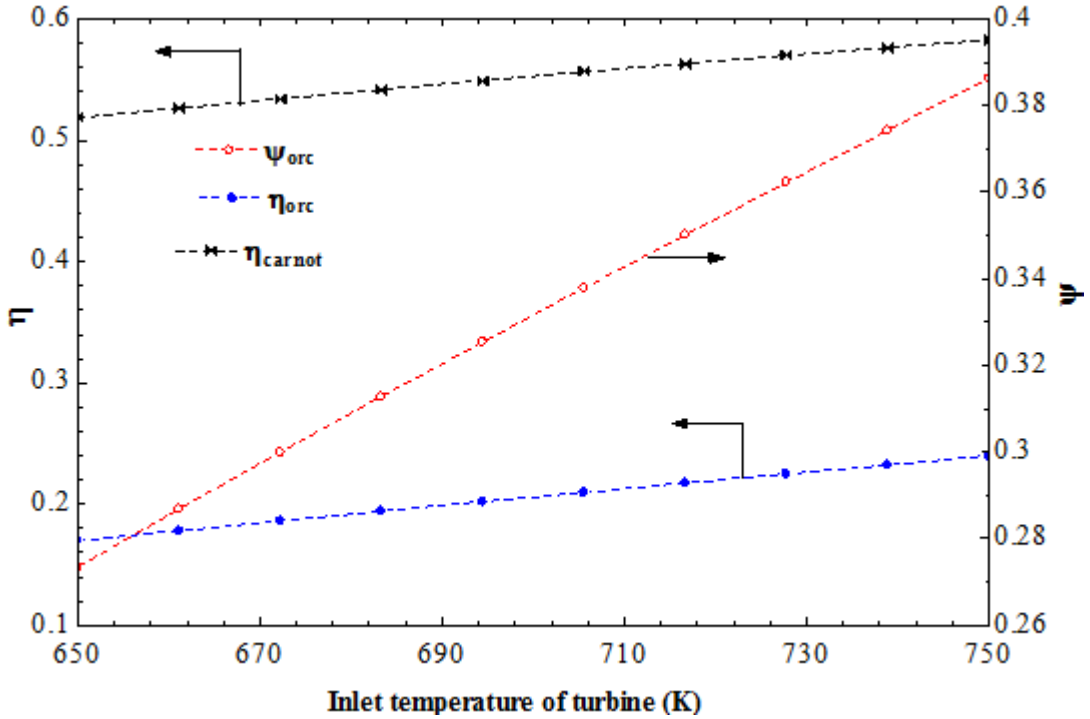

Figure 5.2. Effect of turbine inlet temperature on energetic and exergetic efficiency of ORC and Carnot efficiency

5.3 Effect of Turbine Outlet Temperature on ORC Efficiencies

Figure 5.3 represent the effect of the outlet temperature of the turbine on the ORC energy efficiency and ORC exergy efficiency. It is shown that an increase in the outlet temperature of the turbine causes a decrease in the ORC efficiencies. It can be seen that when the outlet temperature goes from 580 (K) to 640 (K) the ORC energy efficiency decreases from near 39% to 19.73%. Also, by raising the turbine outlet temperature, the exergy efficiency of ORC decreases from about 39% to 19.73%. It is because of the rise in the amount of outlet enthalpies that causes a reduction in the work done in the turbine outlet.

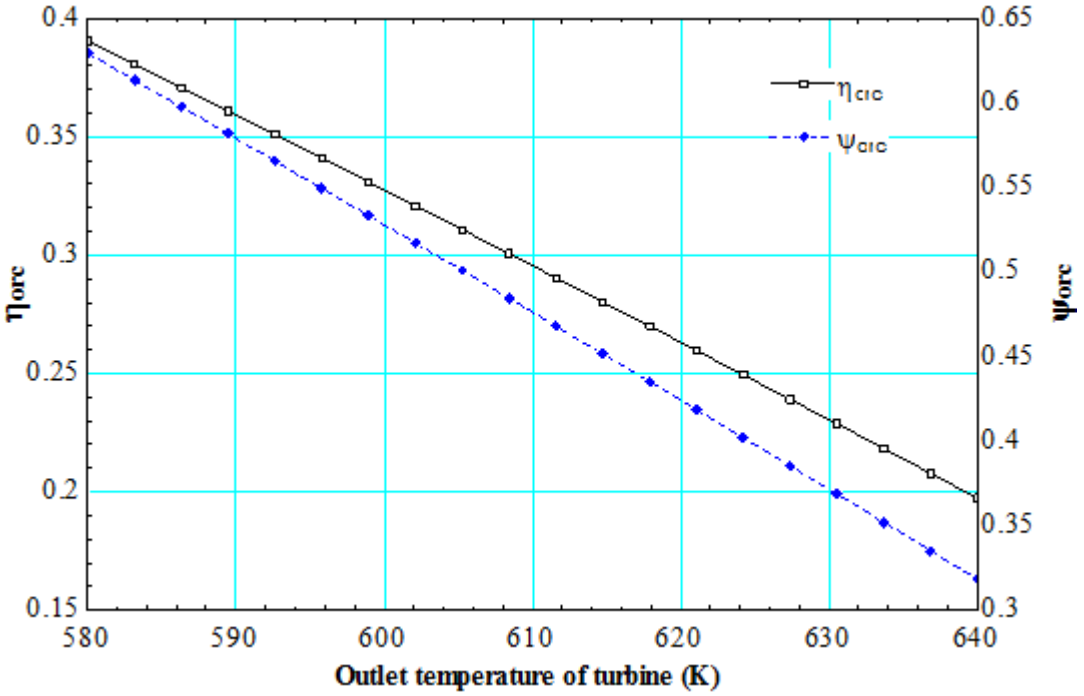

Figure 5.3. Effect of turbine outlet temperature on ORC efficiencies

5.4 Effect of Turbine Inlet Pressure on ORC Efficiencies

The effect of changing the turbine inlet pressure on the ORC energy efficiencies is shown in Figure 5.4. Overall, it can be seen that by increasing the inlet pressure of turbine, both energy and exergy efficiency of Organic Rankine Cycle decreases. When the turbine inlet pressure grows from 10 (kPa) to 2000 (kPa) the ORC energy efficiency decreases from about 21% to near 15% and the ORC exergy efficiency declines from around 34% to 24.33%. This is because increasing the input pressure needs more inlet work for the pump.

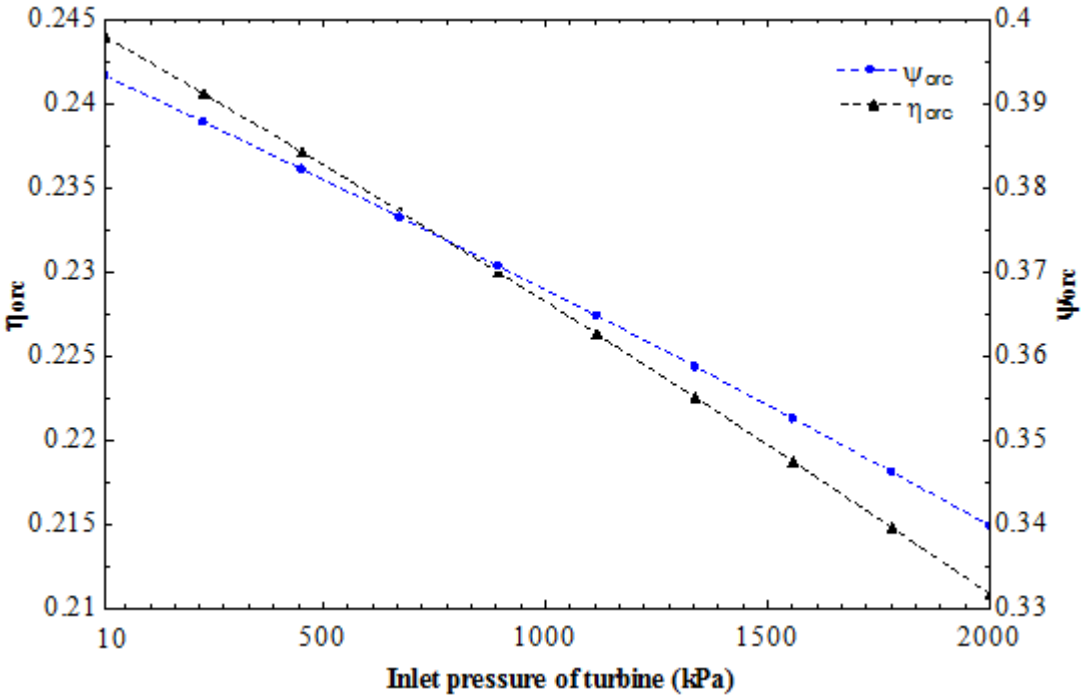

Figure 5.4. Effect of turbine inlet pressure on energetic and exergetic efficiency of ORC

5.5 The Effect of Ambient Temperature on Total Exergy Destruction Rate and Total Exergy Efficiency

Figure 5.5 illustrates the effect of the variation of ambient temperature on total exergy destruction rate and overall exergy efficiency. It can be understood that by raising the temperature from 295 K to 320 K the total exergy destruction of the system is grows from about 2311(kW) to 2793 (kW) while the overall exergy efficiency of the system decreases from 60.94% to 31.47 %.These results are expected since the overall exergy efficiency and total exergy destruction rates are usually inversely proportional properties.

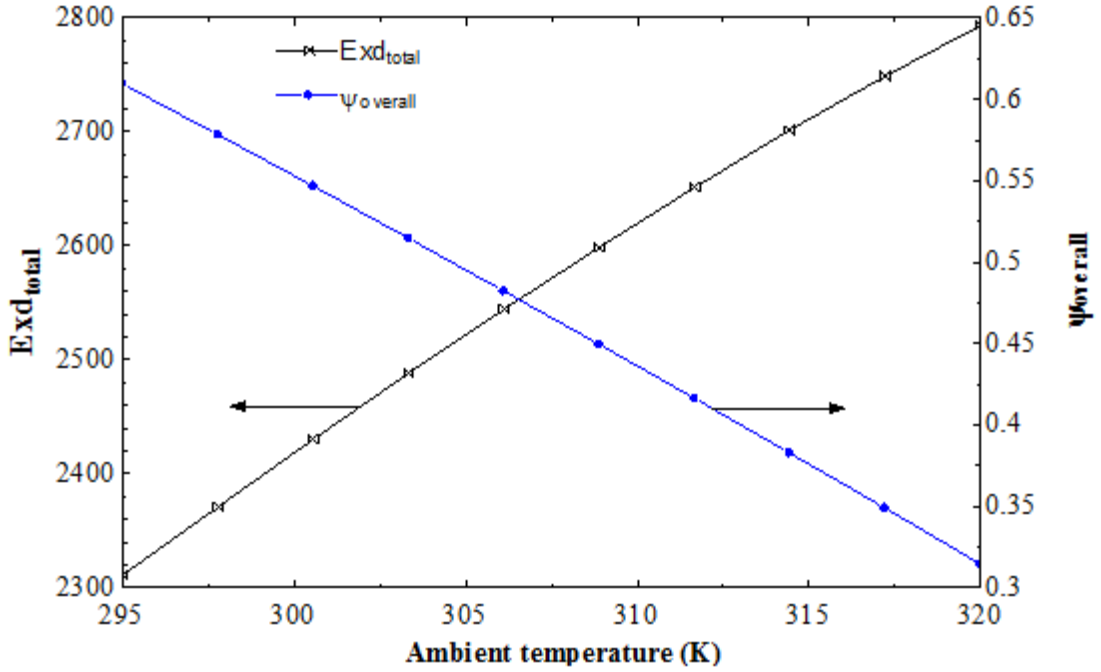

Figure 5.5. The effect of ambient temperature on total exergy destruction rate and total exergy efficiency

5.6 Effect of Ambient Temperature on the COPs

The effect of changing the ambient temperature on the energetic COP and exergetic COP is shown in Figure 5.6. It can be seen that, when the ambient temperature increases, the exergetic COP is grows. This is due to the temperature differences between the system and environment which decreases. It can be seen that by increasing the mass flow, the ORC exergy efficiency grows at a temperature of 295 K , this are 0.1955, 0.1815, 0.1691 for mass flow rates of 9.6 kg/s ,10kg/s and 10.4 kg/s respectively.

On the other hand, by increasing the temperature there is no direct effect on energetic COP of the system since this is independent of any change in the condition of the reference-ambient. It is obvious that by increasing the mass flow rate the energetic COP is decreased to 1.236, 1.188 and 1.143 for a mass flow rate of 9.6 kg/s, 10 kg/s and 10.4 kg/s respectively.

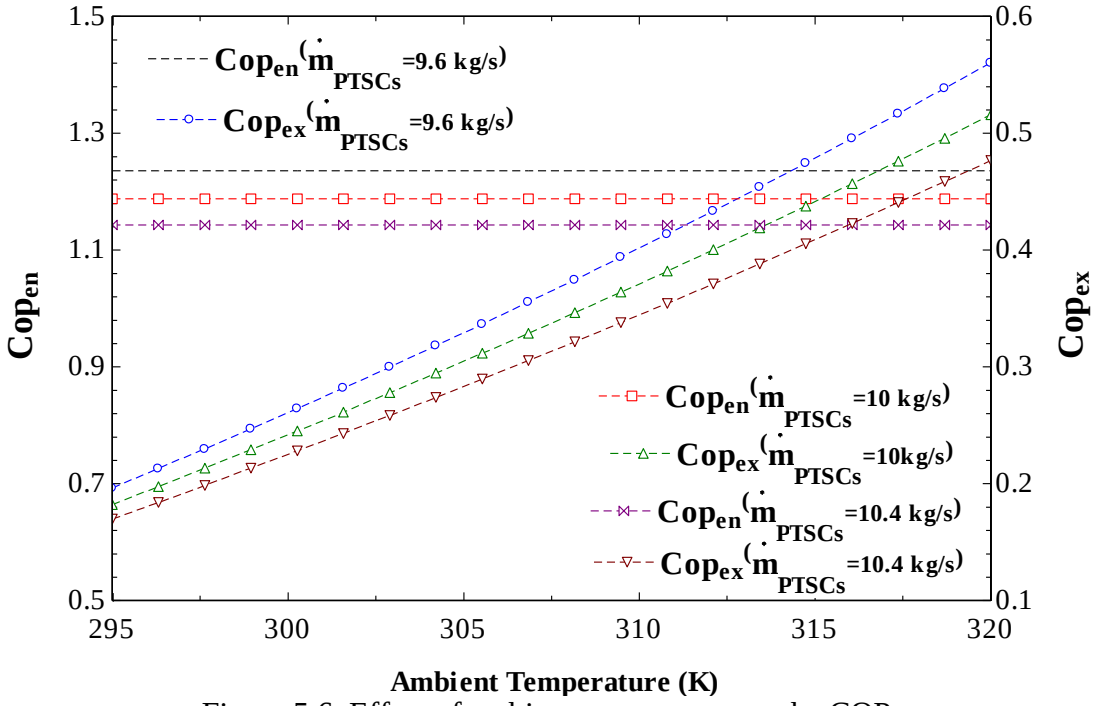

Figure 5.6. Effect of ambient temperature on the COP

5.7 Effect of Ambient Temperature on the Energetic and Exergetic Utilization Factor

Figure 5.7 demonstrates the effect of varying the ambient temperature on the energetic and exergetic utilization factor. It is shown that when the ambient temperature is increasing, the overall exergy efficiency is decreased since the rise in the output temperature is less than the rise in input heat. It can be seen that by increasing the mass flow, the overall exergy efficiency grows at a temperature of 295 K which is 0.5965, 0.6094 and 0.6893 for mass flow rates of 9.6 kg/s ,10kg/s and 10.4 kg/s, respectively.

On the other hand, by increasing the temperature there is no direct effect on utilization factor of the system. Because it doesn't consider the destructions. It is obvious that by increasing the mass flow rate the utilization factor is decreased at

2.715, 2.67 and 2.629 for mass flow rates of 9.6 kg/s, 10 kg/s and 10.4 kg/s, respectively.

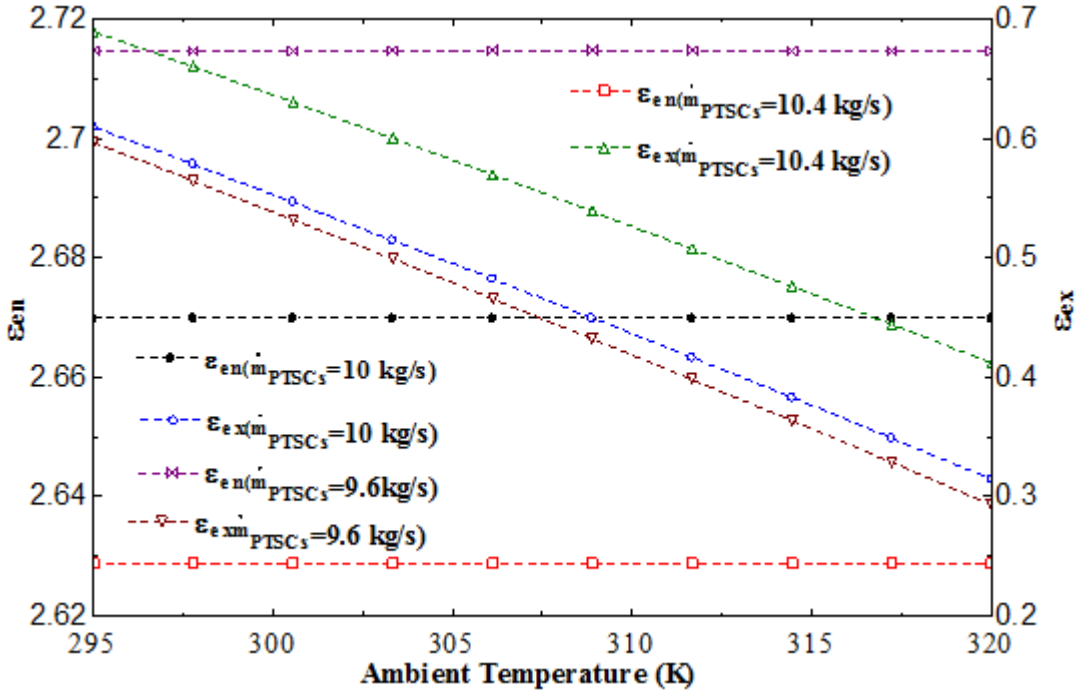

Figure 5.7. Effect of ambient temperature on the utilization factors

5.8 Effect of Inlet Pressure of Turbine on the Turbine Work and Hydrogen Production

The effect of changing the inlet pressure of turbine on the net work produced by turbine and hydrogen production is shown in Figure 5.8. When the inlet pressure of the turbine increases from 10kPa to 2000kPa, both turbine net work and hydrogen production is decreased. This is because by increasing turbine inlet pressure the inlet enthalpy is decreased and this results in a decrease in a net work of the turbine causing the decrease in the amount of hydrogen been produced.

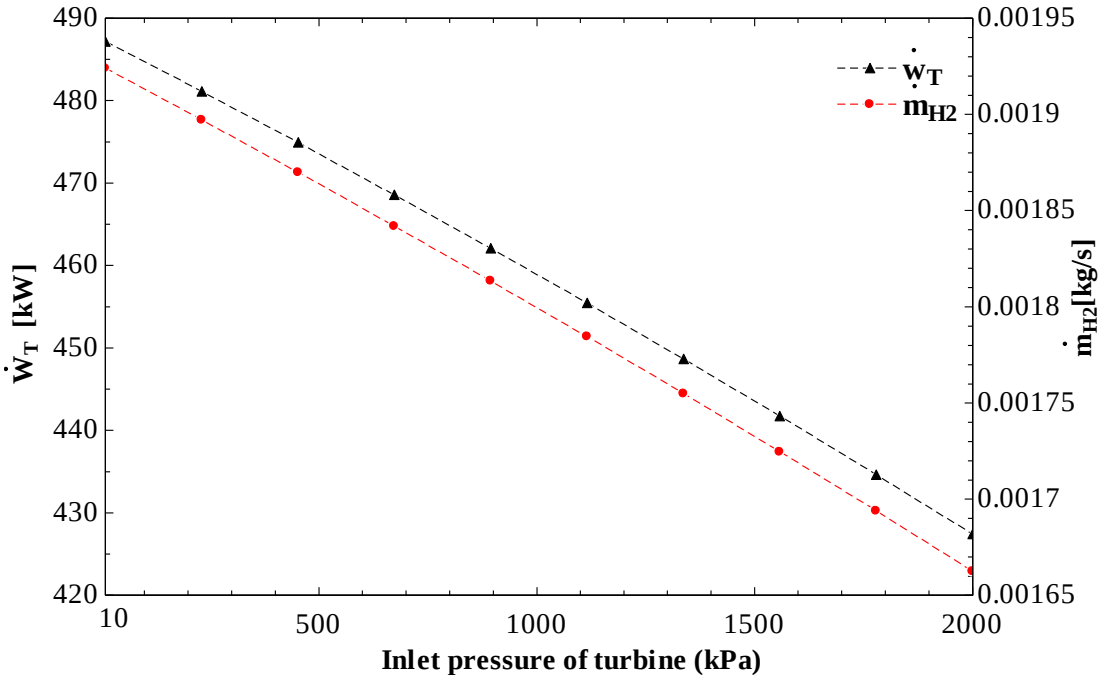

Figure 5.8. Effect of inlet pressure of turbine on the turbine work and hydrogen production

5.9 Effect of Inlet Temperature of Turbine on the Turbine Efficiencies

The Effect of the inlet temperature of the turbine on both the energy and exergy efficiency of the turbine is illustrated in Figure 5.9. Generally, it is clear that by increasing the temperature both energy and exergy efficiency of the turbine is increased but the exergy efficiency of turbine grows with more increased slope. By increasing the temperature from 650K to 750K the energy efficiency of the turbine is increased from near 98.1% to about 98.7 % and the exergy efficiency of the turbine is raised from about 80% to near 90% .This is due to the inlet temperature increment which causes an increase in the input enthalpy and also an increase in the net work of the turbine.

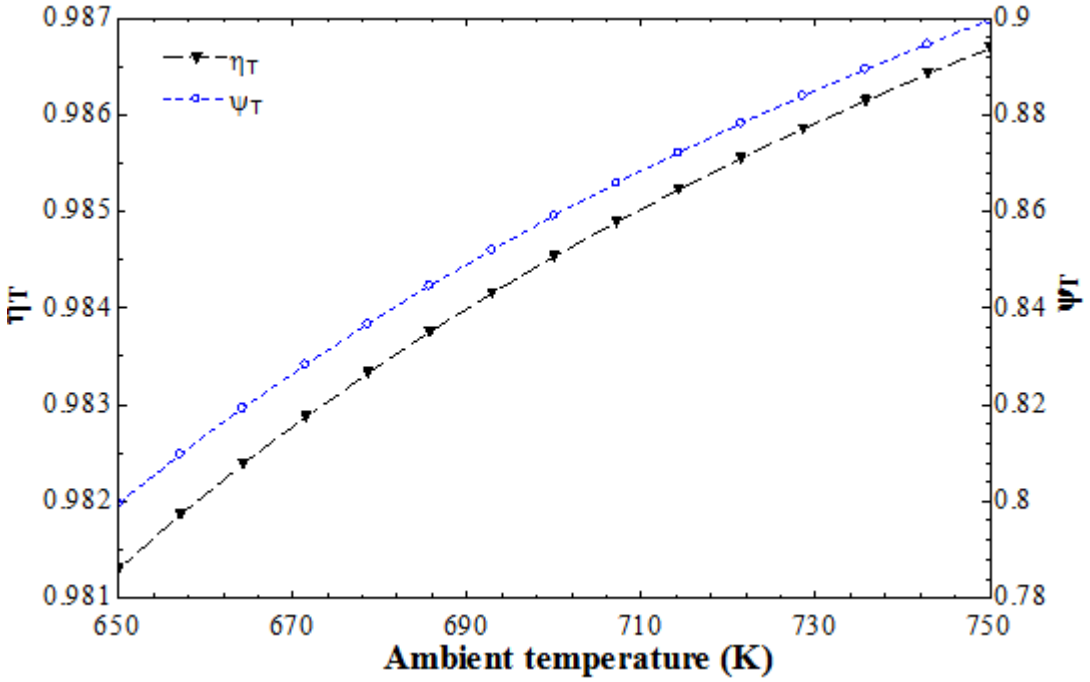

Figure 5.9. Effect of inlet temperature of turbine on the turbine efficiencies

5.10 Effect of Ambient Temperature on the Exergy Destruction Rate of Major Components

Figure 5.10 illustrates the effect of variation of ambient temperature on the exergy destruction rate of major components. The line chart shows that raising the ambient temperature causes growth in the exergy destruction rate of each component. It is clear that by increasing the environmental temperature from 295K to 320K the exergy destruction of condenser 1, condenser 2, evaporator and turbine are increased from ranges of 2.96kW to 3.21 kW, 75.98 kW to 82.42 kW 166.4 kW to 497.9 kW and 58.08 kW to 63.01 kW respectively. This is due to increase in the entropy generation of these sub units because of increase in the finite temperature differences between environmental and operating conditions.

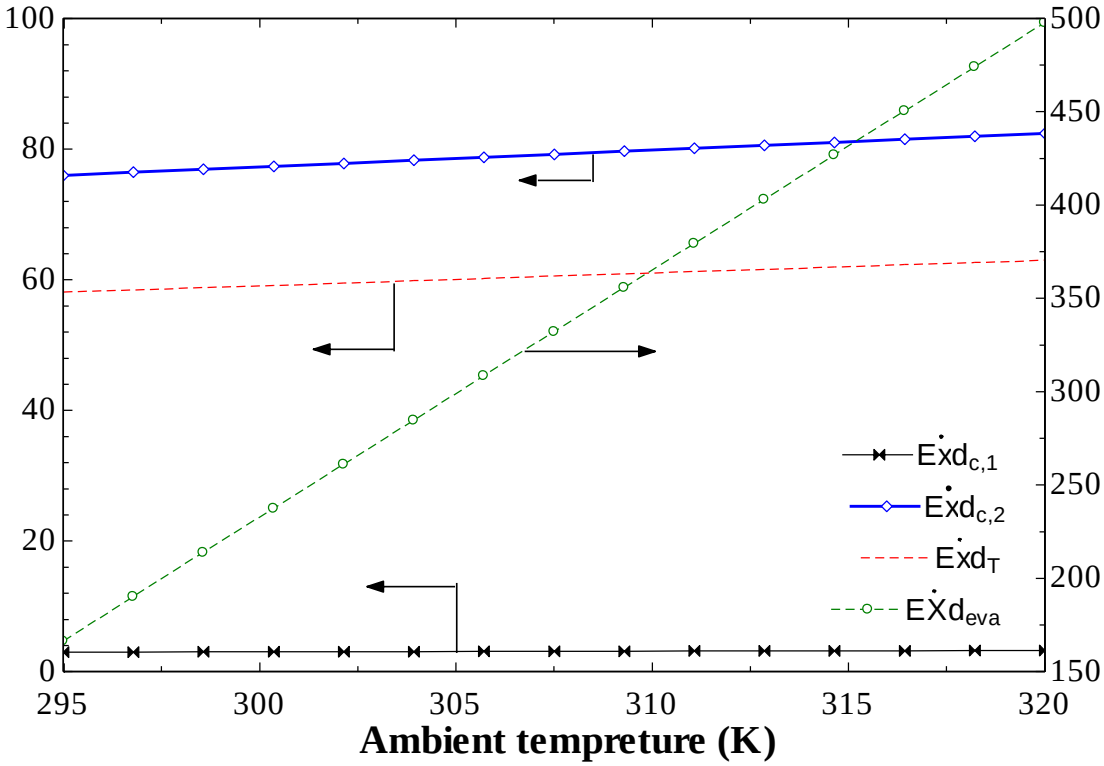

Figure 5.10. Effect of ambient temperature on the exergy destruction rate of major components

5.11 Effect of Steam Generator Heat Transfer Rate on the Turbine Work and Hydrogen Production

The effect of changing steam generator heat transfer rate on the net work produced by turbine and hydrogen production is shown in Figure 5.11. When the steam generator heat transfer rate is increased from 1500kW to 2500 kW, both the turbine net work and hydrogen production is increased. This is because by an increase in the steam generator heat transfer rate, the inlet temperature of the turbine is increased and also the enthalpy is increased and finally the increasing net work of turbine causes the increase in the amount of hydrogen been produced. It is obvious that growing the mass flow has an inverse effect on the net work of turbine and causes a decrease in both turbine net work and the amount of hydrogen produced .The net work of turbine for the steam generator heat transfer rate is 1500kW, 272.6kW,

263.3kW and 249.3kW for ORC mass flow rate of 2.223 kg/s ,2.3kg/s and 2.4 kg/s respectively .

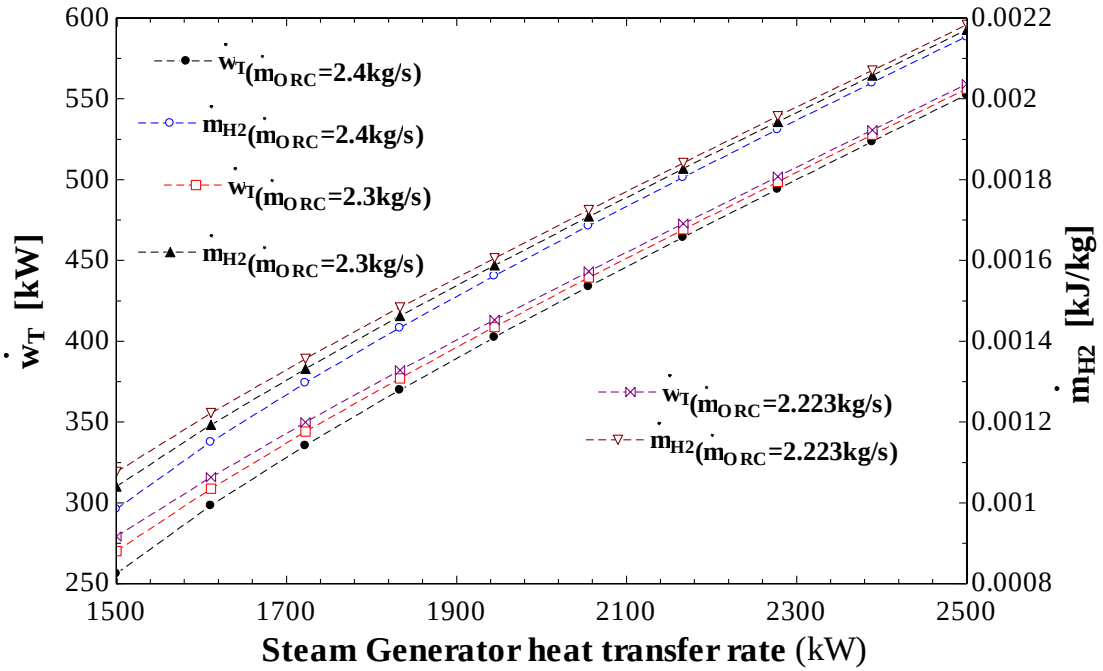

Figure 5.11. Effect of steam generator heat transfer rate on the turbine work and hydrogen production

5.12 The Exergy Destruction Rates

The exergy destruction rates of all the components are demonstrated in Figure 5.12. It can be seen that the majority of system components have a less exergy destruction rate. This is a benefit of the system because we have less heat losses. The first highest destruction rate is in the electolyzer which is 1457 kW. This is due to a chemical reaction in the electrolyzer. Second highest destruction rate is in the high temperature generator. This is as a result of high temperature in these components. In order to gain a higher efficient system, the high exergy destruction rate in electrolyzer should be reduced by decrease the ambient temperature. On the other hand pumps and LTH has the least exergy destruction rates by which these low exergy destruction rates can be helpful in providing the high efficient system.

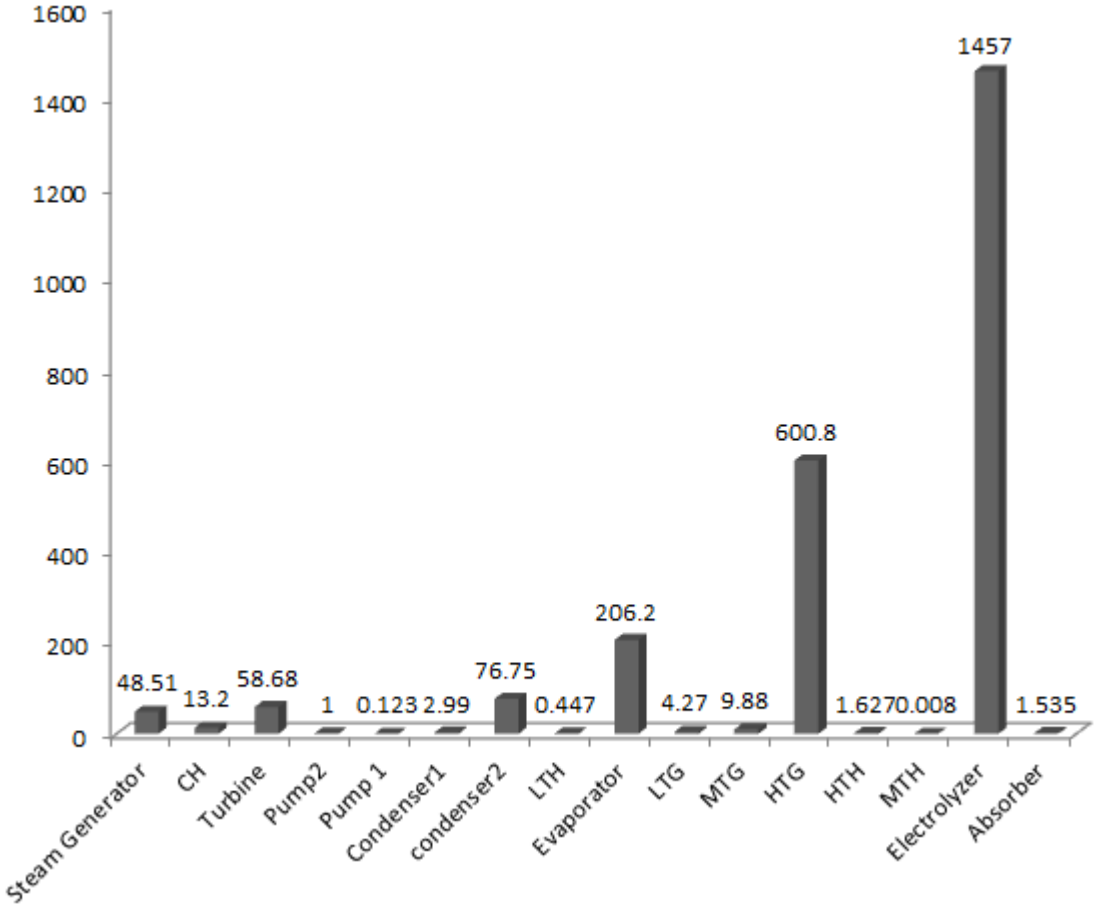

Figure 5.12. The exergy destruction rates (kW)

5.13 Effect of Evaporator Temperature on the Energetic and Exergetic COPs

Figure 5.13 is a demonstrated effect of an evaporator temperature on the energetic and exergetic COP. It is clear that by increasing the evaporator temperature there is no direct effect on the energetic COP because it does not consider the losses. On the other and by growing the evaporator temperature the exergetic COP decreases. It is because the rise in the evaporator temperature causes a decrease in the evaporated heat transfer rate.

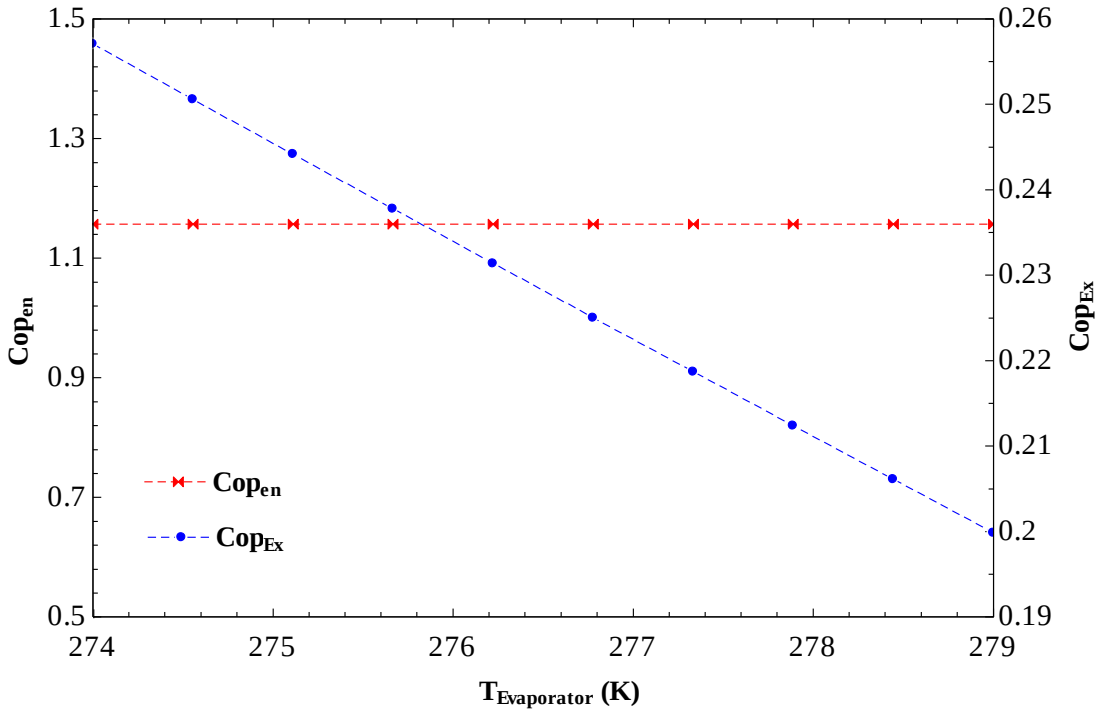

Figure 5.13. Effect of evaporator temperature on the energetic and exergetic COPs

5.14 Exergoenvironmental Analysis

Effect of ambient temperature on the exergoenvironmental indexes is shown in figure 5.14. By increasing the ambient temperature exergoenvironmental impact factor (f_{ei}) is increasing because of more rise in the total exergy destruction compare to input exergy rate. It causes an increase in the exergoenvironmental impact index (θ_{ei}) and a decrease in the exergoenvironmental impact improvement (θ_{eii}) and exergetic sustainability index (θ_{est}). So this system in a place with low ambient temperature is more environmental-friendly.

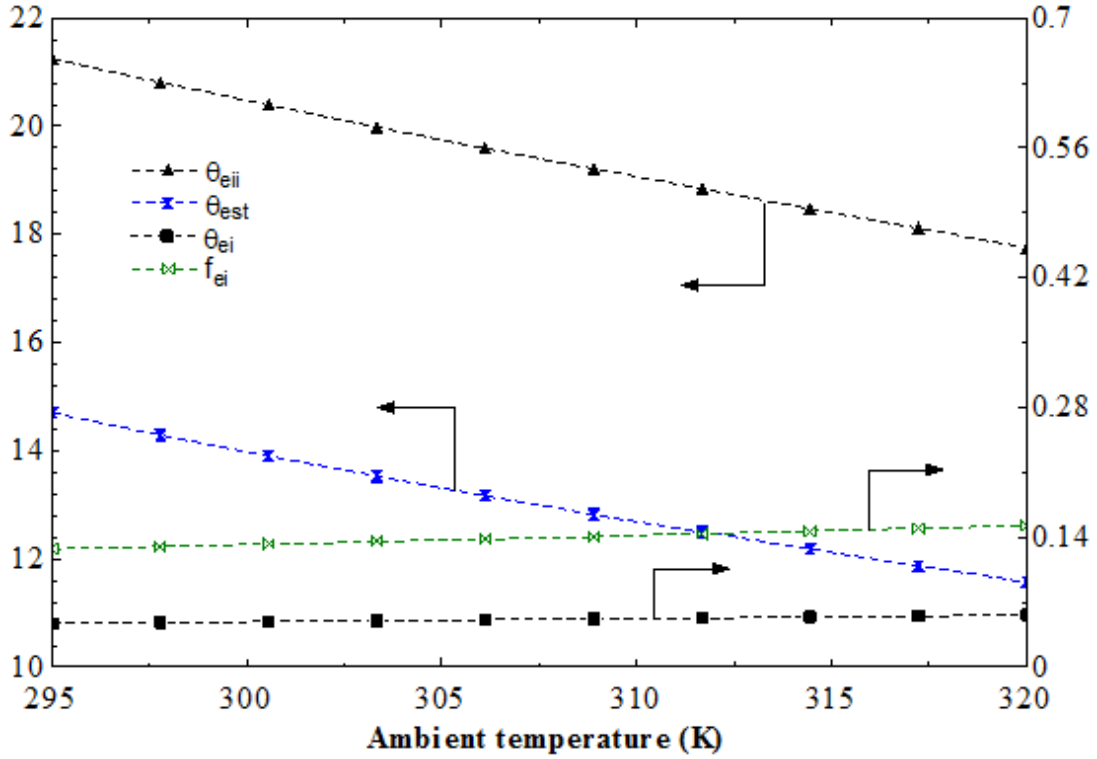

Figure 5.14. Effect of ambient temperature on the exergoenvironmental indexes

Chapter 6

CONCLUSION

Multi-generation energy process attracts much attention because of its production of cooling, heating, hot water, hydrogen, electricity, and dry air from the renewable energy source. This thesis concentrates on developing a new multi-generation energy system using solar energy to supply the energy demand of a residential sector such as a hotel. Energy and exergy analysis of the systems are meant to achieve a better vision into this study. The system utilizes an organic Rankine cycle, an electrolyzer, an absorption chiller and a dryer. The main outputs of the system are electricity, hot water, heating, cooling, dry air, and hydrogen production. A triple effect absorption system is selected to increase efficiency in the cooling and heating system. All modeling is done by Engineering Equation Solver (EES) software. The effects of ambient temperature, mass flow rates of PTSCs and ORC, inlet and outlet temperature of the turbine, inlet and outlet pressure of turbine and heat transfer rate of steam generator are assessed on system efficiencies, ORC efficiencies and amount of generating production and the results are as follow:

- The system has exergetic utilization factor of 60% and energetic utilization factor of 2.62.
- The energetic and exergetic COP of the system are found to be 1.16 and 0.24 respectively.
- The energetic and exergetic of ORC are determined to be 21.08 % and around 34 % respectively.

- The turbine work output is calculated to be 427 kW and the work needed for pumps is determined to be around 6 kW, so the net work is found to be 420.9 kW.
- The cooling effect is 1872 kW which includes 515 kW for drying air and heating effect is 2802 kW which is meant for using hot water and heating the place.
- The system can produce maximum of 0.001662 kg/s hydrogen.

This system can be used in future in residential building and in average it can supply electricity, cooling and heating process to about 600 houses. It is important to note that the remained electricity can be captured in form of hydrogen and then can be recovered to electricity by the fuel cells. In order to produce more cooling, the system should be developed for using in places which have warm weather.

The results of the study should be utilized to develop this system or design new multi-generation system to gain better results in the future. The proposed system should be built and tested experimentally. In order to achieve higher efficiency, other types of renewable energy sources such as biomass and geothermal should be integrated into the current system depending on the local availability of resources.

REFERENCES

[1] International Energy Agency. (2011 November 9). Retrieved from https://www.iea.org

[2] Marland, G., Boden, T. A., Andres, R. J., Brenkert, A. L., & Johnston, C. A. (2007). Global, regional, and national fossil fuel CO2 emissions. *Trends: A Compendium of Data on Global Change*, 37831-6335.

[3] Ratlamwala, T. A. H., & Dincer, I. (2013). Performance assessment of solar-based integrated Cu–Cl systems for hydrogen production. *Solar Energy*, 95, 345-356.

[4] Ahmadi, P., Dincer, I., & Rosen, M. A. (2013). Development and assessment of an integrated biomass-based multi-generation energy system. *Energy*, 56, 155-166.

[5] Khalid, F., Dincer, I., & Rosen, M. A. (2015). Energy and exergy analyses of a solar-biomass integrated cycle for multigeneration. *Solar Energy*, 112, 290-299.

[6] Ghosh, S., & Dincer, I. (2014). Development and analysis of a new integrated solar-wind-geothermal energy system. *Solar Energy*, 107, 728-745.

[7] Atikol, U., Abbasoglu, S., & Nowzari, R. (2013). A feasibility integrated approach in the promotion of solar house design. *International Journal of Energy Research*, 37(5), 378-388.

[8] Al-Sulaiman, F. A., Hamdullahpur, F., & Dincer, I. (2012). Performance assessment of a novel system using parabolic trough solar collectors for combined cooling, heating, and power production. *Renewable Energy*, 48, 161-172.

[9] Cengel, Y. A., & Boles, M. A. (2011). Refrigeration cycles. *Thermodynamics: An Engineering Approach, 7th ed. New York: McGraw-Hill*, 590.

[10] Rabl, A. (1985). Active solar collectors and their applications. *Oxford University Press on Demand.*

[11] Lovegrove, K., & Stein, W. (Eds.). (2012). *Concentrating solar power technology: principles, developments and applications*. Elsevier.

[12] Delisle, V., & Kummert, M. (2014). A novel approach to compare building-integrated photovoltaics/thermal air collectors to side-by-side PV modules and solar thermal collectors. *Solar Energy*, 100, 50-65.

[13] Kodama, T., & Gokon, N. (2007). Thermochemical cycles for high-temperature solar hydrogen production. *Chemical reviews*, 107(10), 4048-4077.

[14] Ghandehariun, S., Rosen, M. A., Naterer, G. F., & Wang, Z. (2011). Comparison of molten salt heat recovery options in the Cu–Cl cycle of hydrogen production. *International journal of hydrogen energy*, 36(17), 11328-11337.

[15] Fernández-García, A., Zarza, E., Valenzuela, L., & Pérez, M. (2010). Parabolic-trough solar collectors and their applications. *Renewable and Sustainable Energy Reviews*, 14(7), 1695-1721.

[16] Kalogirou, S. A. (2004). Solar thermal collectors and applications. *Progress in energy and combustion science*, 30(3), 231-295.

[17] Kalogirou, S. A. (2005). Seawater desalination using renewable energy sources. *Progress in energy and combustion science*, 31(3), 242-281.7

[18] Kaviri, A. G., Jafar, M. M., Tholudin, M. L., & Sharifishourabi, G. (2013). Modelling and exergoeconomic based design optimisation of combined power plants. *International Journal of Exergy*, *13*(2), 141-158.

[19] Tang, T., Villareal, L., & Green, J. (1998). Absorption chillers: Southern California gas company new building institute advanced design guideline series. *New Building Institute*.

[20] Gomri, R. (2010). Investigation of the potential of application of single effect and multiple effect absorption cooling systems. *Energy Conversion and Management*, 51(8), 1629-1636.

[21] Al-Sulaiman, F. A., Dincer, I., & Hamdullahpur, F. (2011). Exergy modeling of a new solar driven trigeneration system. *Solar Energy*, 85(9), 2228-2243.

[22] Ratlamwala, T. A. H., Gadalla, M. A., & Dincer, I. (2011). Performance Assessment of a Combined PEM Fuel Cell and Triple Effect Absorption Cooling System for Cogeneration Applications. *Fuel Cells*, 11(3), 413-423.

[23] Ratlamwala, T. A. H., Dincer, I., & Gadalla, M. A. (2012). Performance analysis of a novel integrated geothermal-based system for multi-generation applications. *Applied Thermal Engineering*, 40, 71-79.

[24] Ozturk, M., & Dincer, I. (2013). Thermodynamic analysis of a solar-based multi-generation system with hydrogen production. *Applied Thermal Engineering*, 51(1), 1235-1244.

[25] Ratlamwala, T. A. H., & Dincer, I. (2013). Development of a geothermal based integrated system for building multigenerational needs. *Energy and Buildings*, 62, 496-506.

[26] Ozturk, M., & Dincer, I. (2013). Thermodynamic assessment of an integrated solar power tower and coal gasification system for multi-generation purposes. *Energy Conversion and Management*, 76, 1061-1072.

[27] Ahmadi, P., Dincer, I., & Rosen, M. A. (2013). Performance assessment and optimization of a novel integrated multigeneration system for residential buildings. *Energy and Buildings*, 67, 568-578.

[28] Ahmadi, P., Dincer, I., & Rosen, M. A. (2014). Multi-objective optimization of a novel solar-based multigeneration energy system. *Solar Energy*, 108, 576-591.

[29] Zamfirescu, C., & Dincer, I. (2014). Assessment of a new integrated solar energy system for hydrogen production. *Solar Energy*, 107, 700-713.

[30] Bicer, Y., & Dincer, I. (2015). Development of a multigeneration system with underground coal gasification integrated to bitumen extraction applications for oil sands. *Energy Conversion and Management*, 106, 235-248.

[31] Islam, S., Dincer, I., & Yilbas, B. S. (2015). Energetic and exergetic performance analyses of a solar energy-based integrated system for multigeneration including thermoelectric generators. *Energy*, 93, 1246-1258.

[32] Bicer, Y., & Dincer, I. (2015). Energy and exergy analyses of an integrated underground coal gasification with SOFC fuel cell system for multigeneration including hydrogen production. *International Journal of Hydrogen Energy*, 40(39), 13323-13337.

[33] Malik, M., Dincer, I., & Rosen, M. A. (2015). Development and analysis of a new renewable energy-based multi-generation system. *Energy*, 79, 90-99.

[34] Al-Sulaiman, F. A., Dincer, I., & Hamdullahpur, F. (2012). Energy and exergy analyses of a biomass trigeneration system using an organic Rankine cycle. *Energy*, 45(1), 975-985.

[35] Dincer, I., & Rosen, M. A. (2012). *Exergy: energy, environment and sustainable development.* Newnes.

APPENDIX

Appendix A: Engineering Equation Solver Codes

"LTH"

m_dot[3]*h[3]=m_dot[19]*h[19]+Q_dot_LTH

ex_dot_LTH=Q_dot_LTH*(1-T[0]/T_LTH)

ex_dot[14]+ex_dot[19]=ex_dot[15]+ex_dot[3]+Exd_dot_LTH

T_LTH=(T[19]+T[3])/2

"CH"

m_dot[17]*h[17]+Q_dot_CH=m_dot[18]*h[18]

ex_dot_CH=Q_dot_CH*(1-T[0]/T_CH)

ex_dot[6]+ex_dot[17]=ex_dot[8]+ex_dot[18]+Exd_dot_CH

T_CH=(T[17]+T[18])/2

"Turbine"

m_dot[33]*(h[33]-h[34])=w_dot_T

ex_dot[33]=ex_dot[34]+w_dot_T+Exd_dot_T

"condenser 1"

m_dot[35]*(h[35]-h[36])=Q_dot_c_1

ex_dot_co_1=Q_dot_c_1*(1-T[0]/T_c_1)

ex_dot[35]=ex_dot[36]+ex_dot_co_1+Exd_dot_c_1

T_c_1=(T[36]+T[35])/2

"condenser 2"

m_dot[7]*h[7]+m_dot[8]*h[8]=m_dot[9]*h[9]+Q_dot_c_2

ex_dot[7]+ex_dot[8]=ex_dot[9]+ex_dot_co_2+Exd_dot_c_2

ex_dot_co_2=Q_dot_c_2*(1-T[0]/T_sc_2)

T_sc_2=(T[7]+T[8]+t[9])/3

"pump1"

w_dot_p_1=m_dot[36]*v[36]*(P[37]-P[36])/eta_p

eta_p =1

ex_dot[36]+w_dot_p_1=ex_dot[37]+Exd_dot_p_1

"pump2"

w_p_2=v[1]*(P[2]-P[1])/eta_p

w_dot_p_2=m_dot[1]*w_p_2

ex_dot[1]+w_dot_p_2=ex_dot[2]*Exd_dot_p_2

"Steam Generator"

m_dot[39]*h[39]=m_dot[38]*h[38]+Q_dot_SG

ex_dot[37]+ex_dot[39]=ex_dot[33]+ex_dot[38]+EXd_dot_SG

ex_dot_SG=Q_dot_SG*(1-T[0]/T_SG)

T_SG=(T[39]+T[38])/2

"eva"

m_dot[10]*h[10]+Q_dot_eva=m_dot[11]*h[11]

ex_dot[10]+Ex_dot_eva=ex_dot[11]+EXd_dot_eva

EX_dot_eva=-(Q_dot_eva*(1-T[0]/T_eva))

t_eva=(t[10]+t[11])/2

"abs"

m_dot[16]*h[16]+m_dot[11]*h[11]=m_dot[1]*h[1]+Q_dot_abs

ex_dot[16]+ex_dot[11]=ex_dot[1]+EX_dot_abs+EXd_dot_abs

EX_dot_abs=Q_dot_abs*(1-T[0]/T_abs)

T_abs=(t[1]+t[11]+t[16])/3

"dryer"

p[48]=p[0]

t[48]=308

w[48]=0.0416

v[48]=Volume(AirH2O,T=T[48],D=DP[48],P=P[48])

dp[48]=DewPoint(AirH2O,T=T[48],w=w[48],P=P[48])

h[48]=Enthalpy(AirH2O,T=T[48],D=DP[48],P=P[48])

s[48]=Entropy(AirH2O,T=T[48],D=DP[48],P=P[48])

ex_dot[48]=m_dotair[48]*((h[48]-h[0])-t[0]*(s[48]-s[0]))

V_dot[48]=5

m_dotair[48]=V_dot[48]/v[48]

t[49]=288

p[49]=p[0]

w[49]=0.022

v[49]=Volume(AirH2O,T=T[49],D=DP[49],P=P[49])

h[49]=Enthalpy(AirH2O,T=T[49],D=DP[49],P=P[49])

dp[49]=DewPoint(AirH2O,T=T[49],w=w[49],P=P[49])

s[49]=Entropy(AirH2O,T=T[49],D=DP[49],P=P[49])

ex_dot[49]=m_dotair[49]*((h[49]-h[0])-t[0]*(s[49]-s[0]))

m_dotair[49]=V_dot[48]/v[49]

p_w=p[49]

t_w=287

hwater=Enthalpy(Water,T=T_w,P=P_w)

s_w=Entropy(Water,T=t_w,P=t_w)

ex_w=m_dotwater*((hwater-h[0])-t[0]*(s_w-s[0]))

m_dot[47]=m_dotwater

eta_dryer=((m_dotair[49]*h[49])/Q_dot_ dryer)

m_dotair[48]*w[48]=m_dotair[49]*w[49]+m_dotwater

Q_dot_eva-Q_dot_cooling=m_dotair[49]*(h[48]-h[49])-m_dotwater*hwater

ex_dot_dehumidificatiin=((1-t[0]/(t[48]))* q_dot_ dryer)

m_dot[48]=m_dotair[48]

m_dot[49]=m_dotair[49]

"Cooling"

Q_dot_cooling=Q_dot_eva-Q_dot_ dryer

EX_dot_cooling=Q_dot_cooling*(1-t[0]/t_cooling)

t_cooling=(t[44]+t[45])/2

"electrolyzer"

etaelec=0.56

w_dot_net=w_dot_t-(w_dot_p_1+w_dot_p_2)

HHV=141800

m_dotH2=(etaelec*w_dot_net)/HHV

W_dot_elec=w_dot_net

p[47]=101

t[47]=25+273

h[47]=Enthalpy(H2,T=T[47])

s[47]=Entropy(H2,T=T[47],P=P[47])

ex_dot[47]=m_dotH2*((h[47]-h[0])-t[0]*(s[47]-s[0]))

exphH2=(h[47]-h[0])-t[0]*(s[47]-s[0])

MW=MolarMass(H2)

exchH2=(235.153*1000)/MW

v[47]=Volume(H2,T=T[47],P=P[47])

exH2=m_dotH2*(exphH2+exchH2)

twater=298

t[46]=twater

pwater=101

p[46]=pwater

h[46]=Enthalpy(Water,T=Twater,P=Pwater)

s[46]=Entropy(Water,T=Twater,P=Pwater)

ex_dot[46]=m_dot[46]*((h[46]-h[0])-t[0]*(s[46]-s[0]))

m_dot[46]=1

exdH2=ex_dot[46]-exH2

"state1"

m_dot[1]=2.4

T[1]=t[2]

p[1]=0.75

x[1]=0.5225

c[1]=Cp_LiBrH2O(T[1],X[1])

ex_dot[1]=m_dot[1]*((h[1]-h[0])-t[0]*(s[1]-s[0]))

h[1]=h_LiBrH2O(T[1],x[1])

s[1]=s_LiBrH2O(T[1],x[1])

rho[1]=rho_LiBrH2O(T[1],X[1])

v[1]=(1/(rho[1]))

s_1=s[1]

"state2"

m_dot[2]=m_dot[1]

T[2]=T[19]+.01

p[2]=2.2

x[2]=x[1]

ex_dot[2]=m_dot[2]*((h[2]-h[0])-t[0]*(s[2]-s[0]))

h[2]=h_LiBrH2O(T[2],x[2])

s[2]=s_LiBrH2O(T[2],x[2])

rho[2]=rho_LiBrH2O(T[2],X[2])

v[2]=(1/(rho[2]))

s_2=s[2]

"state3"

m_dot[3]=m_dot[19]

T[3]=t[20]

c[19]=Cp_LiBrH2O(T[19],X[19])

p[3]=p[2]

x[3]=x[1]

ex_dot[3]=m_dot[3]*((h[3]-h[0])-t[0]*(s[3]-s[0]))

h[3]=h_LiBrH2O(T[3],x[3])

s[3]=s_LiBrH2O(T[3],x[3])

rho[3]=rho_LiBrH2O(T[3],X[3])

v[3]=(1/(rho[3]))

"state4"

m_dot[4]=m_dot[30]

T[4]=Temperature(Water,P=P[4],h=h[4])

p[4]=p[2]

ex_dot[4]=m_dot[4]*((h[4]-h[0])-t[0]*(s[4]-s[0]))

s[4]=Entropy(Water,T=T[4],P=P[4])

v[4]=Volume(water,T=T[4],P=P[4])

m_dot[30]*h[30]=m_dot[4]*h[4]+Q_dot_MTG

t_4=t[4]

P$[4]=Phase$(Water,T=T[4],P=P[4])

"state5"

m_dot[5]=m_dot[4]+m_dot[27]

T[5]=(m_dot[27]*t[27]+m_dot[4]*t[4])/(m_dot[27]+m_dot[4])

p[5]=p[2]

ex_dot[5]=m_dot[5]*((h[5]-h[0])-t[0]*(s[5]-s[0]))

h[5]=Enthalpy(Water,T=T[5],P=P[5])

s[5]=Entropy(Water,T=T[5],P=P[5])

v[5]=Volume(water,T=T[5],P=P[5])

t_5=t[5]

P$[5]=Phase$(Water,T=T[5],P=P[5])

"state6"

m_dot[6]=m_dot[5]

T[6]=Temperature(Water,P=P[6],h=h[6])

p[6]=p[2]

ex_dot[6]=m_dot[6]*((h[6]-h[0])-t[0]*(s[6]-s[0]))

s[6]=Entropy(Water,T=T[6],P=P[6])

v[6]=Volume(water,T=T[6],P=P[6])

m_dot[5]*h[5]=m_dot[6]*h[6]+Q_dot_MTG

t_6=t[6]

P$[6]=Phase$(Water,T=T[6],P=P[6])

"state7"

m_dot[7]=m_dot[22]-m_dot[23]

T[7]=299

p[7]=p[2]

ex_dot[7]=m_dot[7]*((h[7]-h[0])-t[0]*(s[7]-s[0]))

h[7]=Enthalpy(Water,T=T[7],P=P[7])

s[7]=Entropy(Water,T=T[7],P=P[7])

v[7]=Volume(water,T=T[7],P=P[7])

v_7=v[7]

P$[7]=Phase$(Water,T=T[7],P=P[7])

"state8"

m_dot[8]=m_dot[6]

T[8]=Temperature(Water,P=P[8],h=h[8])

p[8]=p[2]

ex_dot[8]=m_dot[8]*((h[8]-h[0])-t[0]*(s[8]-s[0]))

s[8]=Entropy(Water,T=T[8],P=P[8])

v[8]=Volume(water,T=T[8],P=P[8])

m_dot[6]*h[6]=m_dot[8]*h[8]+Q_dot_CH

P$[8]=Phase$(Water,T=T[8],P=P[8])

"state9"

m_dot[9]=m_dot[7]+m_dot[8]

T[9]=292.1

p[9]=p[2]

ex_dot[9]=m_dot[9]*((h[9]-h[0])-t[0]*(s[9]-s[0]))

s[9]=Entropy(Water,T=T[9],P=P[9])

h[9]=Enthalpy(Water,T=T[9],P=P[9])-100

v[9]=Volume(water,T=T[9],P=P[9])

P$[9]=Phase$(Water,T=T[9],P=P[9])

"state10"

m_dot[10]=m_dot[9]

T[10]=275.9

p[10]= p[1]

ex_dot[10]=m_dot[10]*((h[10]-h[0])-t[0]*(s[10]-s[0]))

h[10]=h[9]

s[10]=Entropy(Water,T=T[10],P=P[10])

v[10]=Volume(water,T=T[10],P=P[10])

P$[10]=Phase$(Water,T=T[10],P=P[10])

"state11"

m_dot[11]= m_dot[10]

T[11]=276

p[11]= p[1]

ex_dot[11]=m_dot[11]*((h[11]-h[0])-t[0]*(s[11]-s[0]))

h[11]= Enthalpy(Water,T=T[11],P=P[11])

s[11]=Entropy(Water,T=T[11],P=P[11])

v[11]=Volume(water,T=T[11],P=P[11])

P$[11]=Phase$(Water,T=T[11],P=P[11])

"state12"

m_dot[12]=m_dot[26]-m_dot[27]

T[12]=T[26]+20

p[12]=p[2]

x[12]= 0.5694

ex_dot[12]=m_dot[12]*((h[12]-h[0])-t[0]*(s[12]-s[0]))

h[12]=h_LiBrH2O(T[12],x[12])

s[12]=s_LiBrH2O(T[12],x[12])

rho[12]=rho_LiBrH2O(T[12],X[12])

v[12]=(1/(rho[12]))

"state13"

m_dot[13]=m_dot[32]

T[13]=t[32]-24

p[13]= p[2]

x[13]=x[12]

c[32]=Cp_LiBrH2O(T[32],X[32])

ex_dot[13]=m_dot[13]*((h[13]-h[0])-t[0]*(s[13]-s[0]))

h[13]=h_LiBrH2O(T[13],x[13])

s[13]=s_LiBrH2O(T[13],x[13])

rho[13]=rho_LiBrH2O(T[13],X[13])

v[13]=(1/(rho[13]))

"state14"

m_dot[14]=m_dot[13]+m_dot[23]

T[14]=(m_dot[13]*t[13]+m_dot[23]*t[23])/(m_dot[13]+m_dot[23])

c[14]=Cp_LiBrH2O(T[14],X[14])

x[14]=x[12]

p[14]=p[2]

ex_dot[14]=m_dot[14]*((h[14]-h[0])-t[0]*(s[14]-s[0]))

h[14]=h_LiBrH2O(T[14],x[14])

s[14]=s_LiBrH2O(T[14],x[14])

rho[14]=rho_LiBrH2O(T[14],X[14])

v[14]=(1/(rho[14]))

"state15"

m_dot[15]= m_dot[14]

T[15]= t[14]-Q_dot_LTH/(m_dot[15]*c[14])

p[15]= p[2]

x[15]=x[12]

ex_dot[15]=m_dot[15]*((h[15]-h[0])-t[0]*(s[15]-s[0]))

h[15]=h_LiBrH2O(T[15],x[15])

s[15]=s_LiBrH2O(T[15],x[15])

rho[15]=rho_LiBrH2O(T[15],X[15])

v[15]=(1/(rho[15]))

"state16"

m_dot[16]= m_dot[15]

T[16]= T[15]

p[16]= p[1]

x[16]=x[12]

ex_dot[16]=m_dot[16]*((h[16]-h[0])-t[0]*(s[16]-s[0]))

h[16]=h[15]

s[16]=s_LiBrH2O(T[16],x[16])

rho[16]=rho_LiBrH2O(T[16],X[16])

v[16]=(1/(rho[16]))

"state17"

m_dot[17]= m_dot[1]*0.1

T[17]= t[2]

p[17]= p[2]

x[17]=x[1]

ex_dot[17]=m_dot[17]*((h[17]-h[0])-t[0]*(s[17]-s[0]))

h[17]=h_LiBrH2O(T[17],x[17])

s[17]=s_LiBrH2O(T[17],x[17])

rho[17]=rho_LiBrH2O(T[17],X[17])

v[17]=(1/(rho[17]))

s_17=s[17]

"state18"

m_dot[18]=m_dot[17]

T[18]= t[17]*1.2711

p[18]=p[2]

x[18]=x[1]

c[17]=Cp_LiBrH2O(T[17],X[17])

ex_dot[18]=m_dot[18]*((h[18]-h[0])-t[0]*(s[18]-s[0]))

h[18]=h_LiBrH2O(T[18],x[18])

s[18]=s_LiBrH2O(T[18],x[18])

rho[18]=rho_LiBrH2O(T[18],X[18])

v[18]=(1/(rho[18]))

s_18=s[18]

"state19"

m_dot[19]= m_dot[1]*0.9

T[19]= t[3]-29.7

p[19]=p[2]

x[19]=x[1]

ex_dot[19]=m_dot[19]*((h[19]-h[0])-t[0]*(s[19]-s[0]))

h[19]=h_LiBrH2O(T[19],x[19])

s[19]=s_LiBrH2O(T[19],x[19])

rho[19]=rho_LiBrH2O(T[19],X[19])

v[19]=(1/(rho[19]))

c[3]=Cp_LiBrH2O(T[3],X[3])

"state20"

m_dot[20]=m_dot[3]*0.9

T[20]=t[24]-Q_dot_MTH/(m_dot[20]*c[24])

p[20]=p[2]

x[20]=x[1]

ex_dot[20]=m_dot[20]*((h[20]-h[0])-t[0]*(s[20]-s[0]))

h[20]=h_LiBrH2O(T[20],x[20])

s[20]=s_LiBrH2O(T[20],x[20])

rho[20]=rho_LiBrH2O(T[20],X[20])

v[20]=(1/(rho[20]))

c[24]=Cp_LiBrH2O(T[24],X[24])

"state21"

m_dot[21]=m_dot[3]*0.1

T[21]=t[3]

p[21]=p[2]

x[21]=x[1]

ex_dot[21]=m_dot[21]*((h[21]-h[0])-t[0]*(s[21]-s[0]))

h[21]=h_LiBrH2O(T[21],x[21])

s[21]=s_LiBrH2O(T[21],x[21])

rho[21]=rho_LiBrH2O(T[21],X[21])

v[21]=(1/(rho[21]))

"state22"

m_dot[22]= m_dot[21]+m_dot[18]

T[22]=(t[18]*m_dot[18]+t[21]*m_dot[21])/(m_dot[21]+m_dot[18])

p[22]=p[2]

x[22]=x[1]

ex_dot[22]=m_dot[22]*((h[22]-h[0])-t[0]*(s[22]-s[0]))

h[22]=h_LiBrH2O(T[22],x[22])

s[22]=s_LiBrH2O(T[22],x[22])

rho[22]=rho_LiBrH2O(T[22],X[22])

v[22]=(1/(rho[22]))

"state23"

m_dot[23]=m_dot[22]*0.75

T[23]=t[22]+20

p[23]=p[2]

x[23]=x[12]

ex_dot[23]=m_dot[23]*((h[23]-h[0])-t[0]*(s[23]-s[0]))

h[23]=h_LiBrH2O(T[23],x[23])

s[23]=s_LiBrH2O(T[23],x[23])

rho[23]=rho_LiBrH2O(T[23],X[23])

v[23]=(1/(rho[23]))

v_23=v[23]

"state24"

m_dot[24]= m_dot[20]

T[24]=t[25]

p[24]=p[2]

x[24]=x[1]

c[20]=Cp_LiBrH2O(T[20],X[20])

ex_dot[24]=m_dot[24]*((h[24]-h[0])-t[0]*(s[24]-s[0]))

h[24]=h_LiBrH2O(T[24],x[24])

s[24]=s_LiBrH2O(T[24],x[24])

rho[24]=rho_LiBrH2O(T[24],X[24])

v[24]=(1/(rho[24]))

t_23=t[23]

"state25"

m_dot[25]=m_dot[24]-m_dot[26]

T[25]=t[28]-Q_dot_HTH/(m_dot[28]*c[28])

p[25]= p[2]

x[25]=x[1]

ex_dot[25]=m_dot[25]*((h[25]-h[0])-t[0]*(s[25]-s[0]))

h[25]=h_LiBrH2O(T[25],x[25])

s[25]=s_LiBrH2O(T[25],x[25])

rho[25]=rho_LiBrH2O(T[25],X[25])

v[25]=(1/(rho[25]))

c[28]=Cp_LiBrH2O(T[28],X[28])

"state26"

m_dot[26]=0.1*m_dot[24]

T[26]=T[24]

p[26]= p[2]

x[26]=x[1]

ex_dot[26]=m_dot[26]*((h[26]-h[0])-t[0]*(s[26]-s[0]))

h[26]=h_LiBrH2O(T[26],x[26])

s[26]=s_LiBrH2O(T[26],x[26])

rho[26]=rho_LiBrH2O(T[26],X[26])

v[26]=(1/(rho[26]))

"state27"

m_dot[27]=0.1*m_dot[26]

T[27]=t[12]+10

p[27]= p[2]

ex_dot[27]=m_dot[27]*((h[27]-h[0])-t[0]*(s[27]-s[0]))

h[27]=Enthalpy(Water,T=T[27],P=P[27])

s[27]=Entropy(Water,T=T[27],P=P[27])

v[27]=Volume(water,T=T[27],P=P[27])

P$[27]=Phase$(Water,T=T[27],P=P[27])

"state28"

m_dot[28]=m_dot[25]

T[28]=349.7

c[25]=Cp_LiBrH2O(T[25],X[25])

p[28]= p[2]

x[28]=x[1]

ex_dot[28]=m_dot[28]*((h[28]-h[0])-t[0]*(s[28]-s[0]))

h[28]=h_LiBrH2O(T[28],x[28])

s[28]=s_LiBrH2O(T[28],x[28])

rho[28]=rho_LiBrH2O(T[28],X[28])

v[28]=(1/(rho[28]))

"state29"

m_dot[29]=m_dot[28]-m_dot[30]

T[29]=t[28]*1.04375

p[29]= p[2]

x[29]=x[12]

ex_dot[29]=m_dot[29]*((h[29]-h[0])-t[0]*(s[29]-s[0]))

h[29]=h_LiBrH2O(T[29],x[29])

s[29]=s_LiBrH2O(T[29],x[29])

rho[29]=rho_LiBrH2O(T[29],X[29])

v[29]=(1/(rho[29]))

"state30"

m_dot[30]=0.335*m_dot[28]

T[30]=Temperature(water,P=P[30],h=h[30])

p[30]= p[2]

ex_dot[30]=m_dot[30]*((h[30]-h[0])-t[0]*(s[30]-s[0]))

m_dot[28]*h[28]+Q_dot_HTG=m_dot[30]*h[30]+m_dot[29]*h[29]

s[30]=Entropy(Water,T=T[30],P=P[30])

v[30]=Volume(water,T=T[30],P=P[30])

t_30=t[30]

P$[30]=Phase$(Water,T=T[30],P=P[30])

"state31+"

m_dot[31]=m_dot[29]

T[31]=t[29]-34

p[31]= p[2]

x[31]=x[12]

c[29]=Cp_LiBrH2O(T[29],X[29])

ex_dot[31]=m_dot[31]*((h[31]-h[0])-t[0]*(s[31]-s[0]))

h[31]=h_LiBrH2O(T[31],x[31])

s[31]=s_LiBrH2O(T[31],x[31])

rho[31]=rho_LiBrH2O(T[31],X[31])

v[31]=(1/(rho[31]))

"state32"

m_dot[32]=m_dot[12]+m_dot[31]

T[32]=(m_dot[12]*t[12]+m_dot[31]*t[31])/(m_dot[12]+m_dot[31])

p[32]= p[2]

x[32]=x[12]

ex_dot[32]=m_dot[32]*((h[32]-h[0])-t[0]*(s[32]-s[0]))

h[32]=h_LiBrH2O(T[32],x[32])

s[32]=s_LiBrH2O(T[32],x[32])

rho[32]=rho_LiBrH2O(T[32],X[32])

v[32]=(1/(rho[32]))

"state33+ "

m_dot[33]=2.223

T[33]=t[37]+Q_dot_SG/(m_dot[33]*c[37])

c[37]=Cp(n-Octane,T=T[37],P=P[37])

p[33]=1000

s[33]=Entropy(n-Octane,T=T[33],P=P[33])

h[33]=Enthalpy(n-Octane,T=T[33],P=P[33])

ex_dot[33]=m_dot[33]*((h[33]-h[0])-t[0]*(s[33]-s[0]))

P$[33]=Phase$(n-Octane,T=T[33],P=P[33])

"cp"

cp[33]=Cp(n-Octane,T=T[33],P=P[33])

cp[34]=Cp(n-Octane,T=T[34],P=P[34])

cp[35]=Cp(n-Octane,T=T[35],P=P[35])

cp[36]=Cp(n-Octane,T=T[36],P=P[36])

cp[37]=Cp(n-Octane,T=T[37],P=P[37])

"state34"

m_dot[34]=m_dot[33]

T[34]=0.89911*T[33]

p[34]=10

h[34]=Enthalpy(n-Octane,T=T[34],P=P[34])

s[34]=Entropy(n-Octane,T=T[34],P=P[34])

ex_dot[34]=m_dot[34]*((h[34]-h[0])-t[0]*(s[34]-s[0]))

v[34]=Volume(n-octane,T=T[34],P=P[34])

P$[34]=Phase$(n-Octane,T=T[34],P=P[34])

"state35"

m_dot[35]=m_dot[33]

T[35]=0.49187*T[33]

p[35]=p[34]

h[35]=Enthalpy(n-Octane,T=T[35],P=P[35])

s[35]=Entropy(n-Octane,T=T[35],P=P[35])

ex_dot[35]=m_dot[35]*((h[35]-h[0])-t[0]*(s[35]-s[0]))

v[35]=Volume(n-octane,T=T[35],P=P[35])

P$[35]=Phase$(n-Octane,T=T[35],P=P[35])

"state36"

m_dot[36]=m_dot[33]

T[36]=40+273

p[36]=p[34]

s[36]=Entropy(n-Octane,T=T[36],P=P[36])

h[36]=Enthalpy(n-Octane,T=T[36],P=P[36])

ex_dot[36]=m_dot[36]*((h[36]-h[0])-t[0]*(s[36]-s[0]))

v[36]=Volume(n-octane,T=T[36],P=P[36])

P$[36]=Phase$(n-Octane,T=T[36],P=P[36])

"state37"

m_dot[37]=m_dot[33]

T[37]=T[36]

p[37]=p[33]

s[37]=Entropy(n-Octane,T=T[37],P=P[37])

h[37]=Enthalpy(n-Octane,T=T[37],P=P[37])

ex_dot[37]=m_dot[37]*((h[37]-h[0])-t[0]*(s[37]-s[0]))

v[37]=Volume(n-octane,T=T[37],P=P[37])

P$[37]=Phase$(n-Octane,T=T[37],P=P[37])

"state38"

m_dot[38]=10

T[38]=720

p[38]=101.3

h[38]=Enthalpy('Salt(60NaNO3_40KNO3)', T=T[38], P=P[38])

s[38]=Entropy('Salt(60NaNO3_40KNO3)', T=T[38])

ex_dot[38]=m_dot[38]*((h[38]-h[0])-t[0]*(s[38]-s[0]))

"state39 "

m_dot[39]=m_dot[38]

T[39]=850

p[39]=p[38]

h[39]=Enthalpy('Salt(60NaNO3_40KNO3)', T=T[39], P=P[39])

s[39]=Entropy('Salt(60NaNO3_40KNO3)', T=T[39])

ex_dot[39]=m_dot[39]*((h[39]-h[0])-t[0]*(s[39]-s[0]))

"state40"

m_dot[40]=5

T[40]= 293

p[40]= 101.3

ex_dot[40]=m_dot[40]*((h[40]-h[0])-t[0]*(s[40]-s[0]))

h[40]=Enthalpy(Water,T=T[40],P=P[40])

s[40]=Entropy(Water,T=T[40],P=P[40])

v[40]=Volume(water,T=T[40],P=P[40])

"state41"

m_dot[41]=m_dot[40]

T[41]=Temperature(Water,P=P[41],h=h[41])

p[41]= p[40]

ex_dot[41]=m_dot[41]*((h[41]-h[0])-t[0]*(s[41]-s[0]))

s[41]=Entropy(Water,T=T[41],P=P[41])

v[41]=Volume(water,T=T[43],P=P[41])

m_dot[40]*h[40]+Q_dot_c_1=m_dot[41]*h[41]

"state42"

m_dot[42]=20

T[42]= 293

p[42]= 101.3

ex_dot[42]=m_dot[42]*((h[42]-h[0])-t[0]*(s[42]-s[0]))

h[42]=Enthalpy(Water,T=T[42],P=P[42])

s[42]=Entropy(Water,T=T[42],P=P[42])

v[42]=Volume(water,T=T[42],P=P[42])

"state43"

m_dot[43]=m_dot[42]

T[43]=Temperature(Water,P=P[43],h=h[43])

p[43]= p[42]

ex_dot[43]=m_dot[43]*((h[43]-h[0])-t[0]*(s[43]-s[0]))

s[43]=Entropy(Water,T=T[43],P=P[43])

v[43]=Volume(water,T=T[43],P=P[43])

m_dot[42]*h[42]+Q_dot_c_2=m_dot[43]*h[43]

"state44"

m_dot[44]=15

T[44]= 298

p[44]= 101.3

h[44]=Enthalpy(Water,T=T[44],P=P[44])

s[44]=Entropy(Water,T=T[44],P=P[44])

ex_dot[44]=m_dot[44]*((h[44]-h[0])-t[0]*(s[44]-s[0]))

"state45"

m_dot[45]=m_dot[44]

T[45]=Temperature(Water,P=P[45],h=h[45])

p[45]= p[44]

s[45]=Entropy(Water,T=T[45],P=P[45])

"HTG"

m_dot[34]*h[34]=m_dot[35]*h[35]+Q_dot_HTG

ex_dot[34]+ex_dot[28]=ex_dot[35]+ex_dot[29]+ex_dot[30]+Exd_dot_HTG

ex_dot_HTG=Q_dot_HTG*(1-T[0]/T_HTG)

T_HTG=(t[35]+t[34])/2

"MTG"

m_dot[26]*h[26]+Q_dot_MTG=m_dot[12]*h[12]+m_dot[27]*h[27]

ex_dot_MTG=Q_dot_MTG*(1-T[0]/T_MTG)

ex_dot[30]+ex_dot[26]=ex_dot[4]+ex_dot[12]+ex_dot[27]+Exd_dot_MTG

T_MTG=(T[26]+T[12]+t[27])/3

"LTG"

m_dot[22]*h[22]+Q_dot_LTG=m_dot[23]*h[23]+m_dot[6]*h[6]

ex_dot_LTG=Q_dot_LTG*(1-T[0]/T_LTG)

ex_dot[5]+ex_dot[22]=ex_dot[6]+ex_dot[7]+ex_dot[23]+Exd_dot_LTG

T_LTG=(T[22]+T[23]+T[6])/3

"HTH"

m_dot[29]*h[29]=m_dot[31]*h[31]+Q_dot_HTH

ex_dot_HTH=Q_dot_HTH*(1-T[0]/T_HTH)

ex_dot[29]+ex_dot[25]=ex_dot[31]+ex_dot[28]+Exd_dot_HTH

T_HTH=(T[29]+T[31])/2

"MTH"

m_dot[13]*h[13]+Q_dot_MTH=m_dot[32]*h[32]

ex_dot_MTH=Q_dot_MTH*(1-T[0]/T_MTH)

ex_dot[32]+ex_dot[20]=ex_dot[13]+ex_dot[24]+Exd_dot_MTH

T_MTH=(T[13]+T[32])/2

ex_dot[45]=m_dot[44]*((h[45]-h[0])-t[0]*(s[45]-s[0]))

m_dot[44]*h[44]=m_dot[45]*h[45]+Q_dot_cooling

Cop_en=Q_dot_eva/(Q_dot_HTG+w_dot_p_2)

Cop_Ex=EX_dot_eva/(ex_dot_HTG+w_dot_p_2)

eta_orc=(w_dot_T-w_dot_p_1)/(Q_dot_SG)

psi_orc=(w_dot_T-w_dot_p_1)/(Ex_dot_SG)

eta_T=w_dot_net/(m_dot[33]*h[33]-m_dot[34]*h[34])

eta_carnot=1-(t[36]/t[33])

psi_T=w_dot_net/(ex_dot[33]-ex_dot[34])

Q_dot_heating=Q_dot_c_1+Q_dot_c_2

Exd_total=Exd_dot_SG+Exd_dot_T+Exd_dot_c_1+Exd_dot_p_1+Exd_dot_HTG+E
xd_dot_eva+Exd_dot_abs+exdh2

psi_overall=(W_dot_net+EX_dot_cooling+ex_dot_dehumidificatiin+EX_dot_co_1+
EX_dot_co_2+W_dot_elec)/(EX_dot_SG)

epsilon_overall=(W_dot_net+Q_dot_cooling+Q_dot_dryer+Q_dot_c_1+Q_dot_c_2
+W_dot_elec)/(Q_dot_SG)